THE JOURNAL OF PHYSICAL CHEMISTRY B

 VOLUME 113, NUMBER 19, MAY 14, 2009

FEATURE ARTICLE

Beyond Förster Resonance Energy Transfer in Biological and Nanoscale Systems

David Beljonne,[†] Carles Curutchet,[‡] Gregory D. Scholes,*[,‡] and Robert J. Silbey[§]

Laboratory for Chemistry of Novel Materials, Center for Research on Molecular Electronics and Photonics, University of Mons-Hainaut, Place du Parc 20, B-7000 Mons Belgium, Lash-Miller Chemical Laboratories, Institute for Optical Sciences and Centre for Quantum Information and Quantum Control, University of Toronto, 80 St. George Street, Toronto, Ontario, M5S 3H6 Canada, and Department of Chemistry, Massachusetts Institute of Technology, Cambridge, Massachusetts 02139

Received: January 23, 2009; Revised Manuscript Received: February 28, 2009

After photoexcitation, energy absorbed by a molecule can be transferred efficiently over a distance of up to several tens of angstroms to another molecule by the process of resonance energy transfer, RET (also commonly known as electronic energy transfer, EET). Examples of where RET is observed include natural and artificial antennae for the capture and energy conversion of light, amplification of fluorescence-based sensors, optimization of organic light-emitting diodes, and the measurement of structure in biological systems (FRET). Förster theory has proven to be very successful at estimating the rate of RET in many donor−acceptor systems, but it has also been of interest to discover when this theory does not work. By identifying these cases, researchers have been able to obtain, sometimes surprising, insights into excited-state dynamics in complex systems. In this article, we consider various ways that electronic energy transfer is promoted by mechanisms beyond those explicitly considered in Förster RET theory. First, we recount the important situations when the electronic coupling is not accurately calculated by the dipole−dipole approximation. Second, we examine the related problem of how to describe solvent screening when the dipole approximation fails. Third, there are situations where we need to be careful about the separability of electronic coupling and spectral overlap factors. For example, when the donors and/or acceptors are molecular aggregates rather than individual molecules, then RET occurs between molecular exciton states and we must invoke generalized Förster theory (GFT). In even more complicated cases, involving the intermediate regime of electronic energy transfer, we should consider carefully nonequilibrium processes and coherences and how bath modes can be shared. Lastly, we discuss how information is obscured by various forms of energetic disorder in ensemble measurements and we outline how single molecule experiments continue to be important in these instances.

1. Introduction

Förster resonance energy transfer (FRET) is a common and fundamental photophysical process in life and materials sciences. After absorption of light, intrachromophore processes, such as radiative decay (e.g., fluorescence, phosphorescence) and radiationless transitions (e.g., internal conversion, intersystem crossing), dissipate the absorbed energy. FRET is an *interchromophore* relaxation process that transmits the electronic excitation from an initially excited donor to a ground-state acceptor chromophore.[1] The manifestations and uses of FRET are too numerous to list here. Some notable examples include light harvesting in photosynthesis, design of high performance sensors, labeling, structure determination, and photoprotection.

Soon after the initial observations of FRET in chemistry and biology,[2] the concepts underpinning its mechanism were elucidated. First, it was realized that a collision between donor and acceptor is not required to transfer the electronic energy, and that FRET is mediated by a quantum-mechanical coupling between the electronic transitions.[3] This transition dipole−transition dipole interaction depends on the strength of each transition,

[†] University of Mons-Hainaut.
[‡] University of Toronto.
[§] Massachusetts Institute of Technology.

10.1021/jp900708f CCC: $40.75
Published on Web 03/30/2009

David Beljonne is a Research Director of the Belgian National Science Foundation (FNRS). He received his Ph.D. degree from the University of Mons-Hainaut (UMH) in 1994. After postdoctoral stays in Cambridge, U.K. (with Prof. Sir Richard Friend), and Rochester (with Prof. Shaul Mukamel) in 1995, he joined the "Laboratory for Chemistry of Novel Materials" at UMH as a FNRS research fellow. His research interests deal with the modeling using combined classical and quantum-chemical approaches of the nature and dynamics of electronic excitations in nanoscale materials, in relation to their use as active components in opto-electronic applications.

Carles Curutchet was born in Madrid, Spain, in 1977. He received his B.Sc. (1999), M.Sc. (2001), and Ph.D. (2005) degrees from the University of Barcelona and then undertook postdoctoral studies at the University of Pisa (2005) and University of Parma (2006−2007). In 2008, he joined the research group of professor Gregory Scholes at the University of Toronto, where he is now a postdoctoral fellow. His research interests are the theoretical modeling of solvent effects on the structure, properties, and reactivity of chemical systems.

Gregory Scholes is an Associate Professor at the University of Toronto in the Department of Chemistry. He joined the faculty there in 2000. He obtained B.Sc. (Hons.) (1990) and Ph.D. (1994) degrees from the University of Melbourne and then undertook postdoctoral studies at Imperial College in London from 1995 to 1997 as a Ramsay Memorial Research Fellow and at the University of California, Berkeley, from 1997 to 2000. He is presently an NSERC EWR Steacie Fellow. His present research focuses on elucidating the principles deciding electronic structure, optical properties, and reactions of nanoscale systems by combining synthesis, theory, and ultrafast laser spectroscopy.

Robert Silbey is a Professor of Chemistry at Massachusetts Institute of Technology. He received his Ph.D. degree from the University of Chicago in 1965 and then completed a Postdoctoral Fellow at the University of Wisconsin. He was chair of MIT's Department of Chemistry from 1990 to 1995, the Director of MIT's Center for Materials Science and Engineering from 1998 to 2000, and Dean of the School of Science from 2000 to 2007. His research interests deal with theoretical chemistry, relaxation and coherence in low temperature systems, spectroscopy of molecules in glasses and solids, single molecule spectroscopy, vibronic interactions in molecules and solids, highly vibrationally excited polyatomic molecules, and electronic and optical properties of polymers.

and it diminishes with the cube of donor−acceptor separation (R), yielding the well-known $1/R^6$ distance dependence of FRET. It was next established that energy conservation during FRET is ensured by spectral overlap between donor emission and acceptor absorption.[4] Förster brought these ideas together in a theory that connected the FRET rate (or efficiency) with parameters gathered from spectroscopic measurements of the donor and acceptor chromophores.[5]

Despite the success of FRET theory for predicting energy transfer rates and assessing conformational equilibrium configurations (i.e., as a spectroscopic ruler) in a wide variety of systems, it has been of interest to identify when and how FRET theory does not work. Thereby, we can learn more about how chromophores interact on ultrafast time scales and/or at short separation. These phenomena are the subject of this paper. In the case of ultrafast energy transfer, a number of the FRET assumptions need to be revisited, particularly the role of coherent effects (section 5). Deviations from the $1/R^6$ distance dependence of the FRET rate usually occur at closer interchromophore separations when the dipole approximation fails (section 2). Electronic coupling can also be transmitted by through-bond pathways introduced by molecular bridges connecting donor to acceptor (section 4). Recently, it has been found that electronic couplings can acquire additional distance dependence by screening from the environment (section 6). In these cases, the rules for distance dependence and/or optimal interchromophore orientation can be substantially different than those assumed by Förster theory.

FRET is formulated under the assumption that the electronic coupling between donor and acceptor is very weak,[6] so that electronic coupling is the perturbation promoting energy transfer from donor to acceptor. On the other hand, when the electronic coupling is strong, molecular excitons are the primary excited states of the system.[7] Relaxation among these delocalized states is promoted by exciton-bath coupling (not electronic coupling).[8] Theoretical studies have long contemplated intermediate cases whereby the energy is transferred coherently from donor to acceptor, but it is only recently that experimental means to measure the characteristics of this regime have been reported. In section 5, we discuss some of the causes and signatures of coherent energy transfer, and the kinds of experiments that are required to obtain evidence for such phenomena. The reason that researchers are interested in this kind of energy transfer is that, not only is it considered important to understand the nature of quantum transport in multichromophoric assemblies, but control of such dynamics might permit highly efficient long-range energy migration.

We formalize these statements by writing the FRET rate[9] eq 1a in the equivalent form eq 1b:

$$k_{\mathrm{FRET}} = \frac{1}{\tau_{\mathrm{D}}^0}\left[\frac{R_0}{R}\right]^6 \tag{1a}$$

$$= \frac{2\pi}{\hbar}|sV_{\mathrm{dd}}|^2 J \tag{1b}$$

where τ_{D}^0 is the donor excited-state lifetime, R_0 is the Förster critical radius, R is the interchromophore separation, V_{dd} is the electronic coupling in the dipole−dipole approximation, J is a spectral overlap defined in terms of area-normalized donor emission and acceptor absorption spectra, and s is the solvent screening of the electronic coupling (which equals $1/n^2$ in the Förster model, where n is the refractive index of the solvent).

In this article, we will consider four ways that electronic energy transfer is promoted by mechanisms beyond those explicitly considered in FRET theory. First, the important situations when the electronic coupling is not equal to V_{dd}. Second, the related problem of how to describe the solvent screening when the dipole approximation fails, which means that $s \neq 1/n^2$. In these cases, the Fermi golden rule rate expression can still apply and we will refer to energy transfer simply as resonance energy transfer (RET) to differentiate it from the specific case of FRET. Third, there are situations where we need to be careful about the separability of electronic coupling and spectral overlap factors. For example, when the donors and/or acceptors are molecular aggregates rather than individual molecules, then RET occurs between molecular exciton states and we must invoke generalized Förster theory (GFT). In even more complicated cases, involving the intermediate regime of electronic energy transfer, we should consider carefully nonequilibrium processes and coherences. We propose to call any such cases coherent resonance energy transfer (CRET). Lastly, we discuss how information can be hidden by various forms of energetic disorder in ensemble measurements.

2. Failure of the Point-Dipole Approximation

The point-dipole approximation in FRET has the same form as the classical electrostatic interaction between point dipoles, but it is the quantum-mechanical coupling between donor and acceptor transition dipoles μ_{D} and μ_{A} with center-to-center separation R and orientation factor $\kappa = \hat{\mu}_{\mathrm{D}}\cdot\hat{\mu}_{\mathrm{A}} - 3(\hat{\mu}_{\mathrm{D}}\cdot\hat{R})(\hat{\mu}_{\mathrm{A}}\cdot\hat{R})$:[10]

$$V_{\mathrm{dd}} = \frac{1}{4\pi\varepsilon_0}\frac{\kappa\mu_{\mathrm{D}}\mu_{\mathrm{A}}}{R^3} \tag{2}$$

In the Förster equation, this explicit form of the coupling is hidden by the relationships drawn with spectral quantities. The

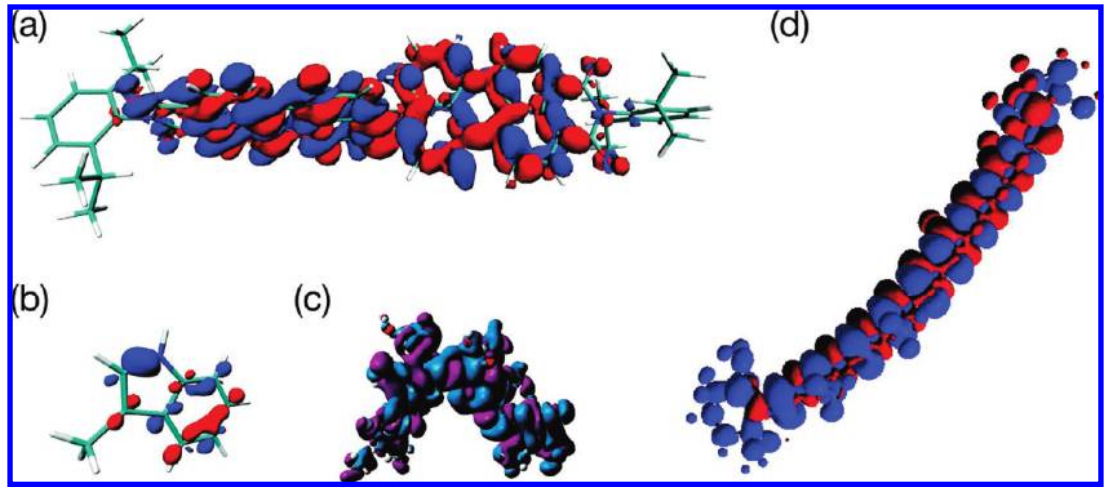

Figure 1. Examples of transition densities calculated using quantum-chemical methods. Note how they follow the shape of the chromophore in each case. (a) A bis-perylene derivative. (b) Tryptophan. (c) A bilin from cryptophyte photosynthetic antenna systems. (d) The $S_0 \rightarrow S_2$ state of a carotenoid found in photosynthetic proteins.

point-dipole approximation works very well for quantifying the optical spectroscopy of allowed transitions because the wavelength of light is long compared to the size of a molecule and therefore its oscillating electric field averages over details of the molecular wave function.[11] Such an averaging does not happen when a molecule interacts with a nearby molecular neighbor.[12] In fact, it is even possible for optically dark transitions to mediate RET effectively.[13] That is because these donor and acceptor molecules see each other's shape in the form of transition densities, not transition dipoles. A transition density, defined as $\rho_{eg} = |e\rangle\langle g|$, represents the superposition state of ground (g) and excited (e) states.[14] Examples of transition densities are illustrated in Figure 1.

To calculate the Coulombic coupling accurately, quantum-chemical methods are required. Typical approaches include the transition density cube (TDC) method,[12] the distributed monopole approximation,[15,16] or "line dipole" approximations.[17,18] Systematic studies of how the calculated Coulombic interaction varies with the quality of the quantum-chemical approach used have recently been reported.[19−21] Procedures like the TDC method have enabled researchers to obtain important quantitative insights into RET dynamics for systems ranging from photosynthetic proteins[22] to conjugated polymers.[23] Here, we develop a specific example.

Recent experimental studies suggest that photogeneration of charges in donor−acceptor dyads and heterojunctions including fullerenes as acceptors proceed via a two-step mechanism, with RET from the donor to the acceptor *prior* to hole migration.[24−29] The design rules for new donors in fullerene-based polymer solar cells, which have so far been solely based on a direct electron transfer reaction process, might thus have to be reconsidered in the light of these new findings. In addition, these results call for a more fundamental question regarding the mechanism for energy transfer that we would like to address here. According to the FRET model, fast resonant energy transfer indeed requires overlap between the donor emission and acceptor absorption spectra combined with strong dipole−dipole coupling between the chromophores. However, because of symmetry selection rules, the local excitations of the C_{60} derivative that are in close resonance with the lowest (emitting) excited state of the donors display small transition dipole moments, a feature that is seemingly at odds with the measured fast (in the ps^{-1} range) energy transfer rates. As a matter of fact, it was shown that the Förster model could only reproduce the energy transfer rate measured in a toluene solution of a tetraphenylenevinylene-*N*-methylfulleropyrrolidine (OPV_4-MPC_{60}) dyad when making the unphysical assumption that the effective distance between the interacting point dipoles is less than half of the actual donor−acceptor center-to-center separation.[25]

We have applied an atomistic model based on a quantum-chemical description of the electronic excitations to study resonant energy transfer in OPV_n-MPC_{60} dyads.[30] Fast (subpicosecond) energy transfer is predicted to take place from the oligophenylenevinylene to the C_{60} derivative, as a result of the presence of multiple pathways involving low-lying excited states of the MPC_{60} acceptor. In addition, we found it essential to go beyond the point-dipole approximation assumed in Förster theory and use a multicentric transition density approach[16,31−33] to obtain a reliable estimate of the electronic couplings mediating the energy hopping process. The shortcoming of the point-dipole model is related to the fact that the actual electronic matrix elements in such dyads are dominated by contributions to the excited-state wave functions arising from the donor and acceptor molecular edges that are in close contact (since these lead to the shortest donor−acceptor interatomic distances). When accounting for all relevant channels in a multicentric transition density approach, energy transfer rates in good agreement with experiment are obtained; see Figure 2 and Table 1.

3. Nanoscale Systems

Recently, much attention has been directed toward understanding RET in nanoscale systems, such as semiconductor nanocrystalline quantum dots (QDs)[34−37] or single-walled carbon nanotubes (SWNTs).[38] In contrast to molecular systems, however, separations between possible donors/acceptors in nanoscale systems are typically similar to, or smaller than, the dimensions of the donor or acceptor themselves, so it becomes necessary to assess to what extent the point-dipole approximation is valid in such systems. Recently, we studied the validity of the point-dipole model in the case of CdSe QDs[39] and SWNTs[40] using atomistic quantum-mechanical methods. The results are quite interesting in light of what we know about molecular RET. The point-dipole model was found to be an excellent method to predict electronic couplings involving QDs. In contrast, the interaction between SWNTs was found to be overestimated by

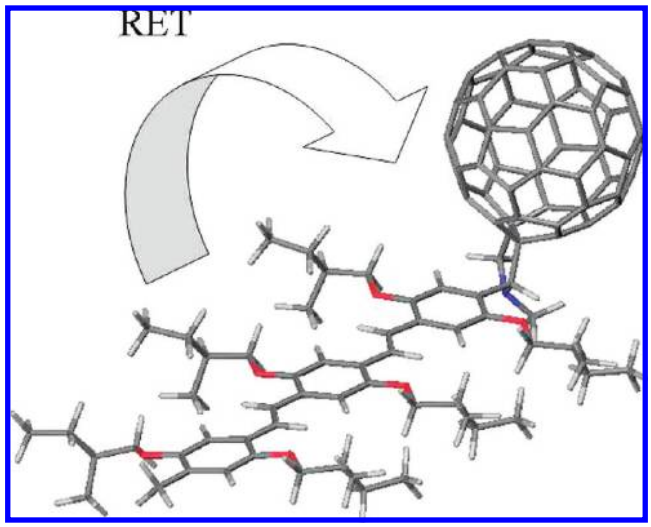

Figure 2. Chemical structure of the OPV_3-MPC_{60} dyad.

TABLE 1: Calculated and Measured Energy Transfer Rates (k_{RET}) in OPV_n-MPC_{60} Dyads (The Numbers in Parentheses Correspond to the Förster Rates and the Point-Dipole Approximation)

	k_{RET} (10^{12} s^{-1})	
dyad	calculated[a]	experiment[b]
OPV_2-MPC_{60}	6.6 (1.1)	2.9
OPV_3-MPC_{60}	2.3 (0.3)	2.1
OPV_4-MPC_{60}	0.5 (0.1)	1.1

[a] See ref 30. [b] See ref 24.

1 order of magnitude at center-to-center tube separations typically found in SWNT bundles (~12−16 Å)—that corresponds to 2 orders of magnitude in the rate!

In Figure 3, we show our results for a pair of 3.9 nm diameter wurtzite CdSe QDs aligned parallel with respect to their crystallographic *c*-axis, and for two parallel (7,5) SWNTs 10 nm in length. Transition densities for the bright states were calculated using the atomistic semiempirical pseudopotential method for the QDs[41] and from time-dependent density functional theory for the SWNTs. Electronic couplings, *V*, were then calculated as a function of the donor−acceptor separation both using the point-dipole model and a multicentric transition density approach.[16,31−33] We found that the point-dipole model works surprisingly well for the QD−QD pair, even at quasi-contact distances (~4 nm). In sharp contrast, the point-dipole approximation strongly overestimates *V* even at separations of several times the tube diameter (e.g., at $R \sim 10$ nm) for the SWNT−SWNT pair. The quasi-spherical symmetry of the QD transition density, which allows an effective averaging onto a point dipole, seems to be the reason for such unexpected behavior. Indeed, it has recently been predicted for CdSe nanorods that the point-dipole approximation is subject to substantially larger errors.[42] Our results confirm the paradigm that the point-dipole model assumed in Förster theory should be avoided when studying electronic energy transfer in *extended* nanoscale systems, such as polyenes (and carotenoids), organic conjugated polymers, inorganic nanorods, or carbon nanotubes.

4. Through-Space versus Through-Bond Electronic Coupling

Through-bond electronic coupling happens when orbitals on each of the donor and acceptor chromophores mix slightly with

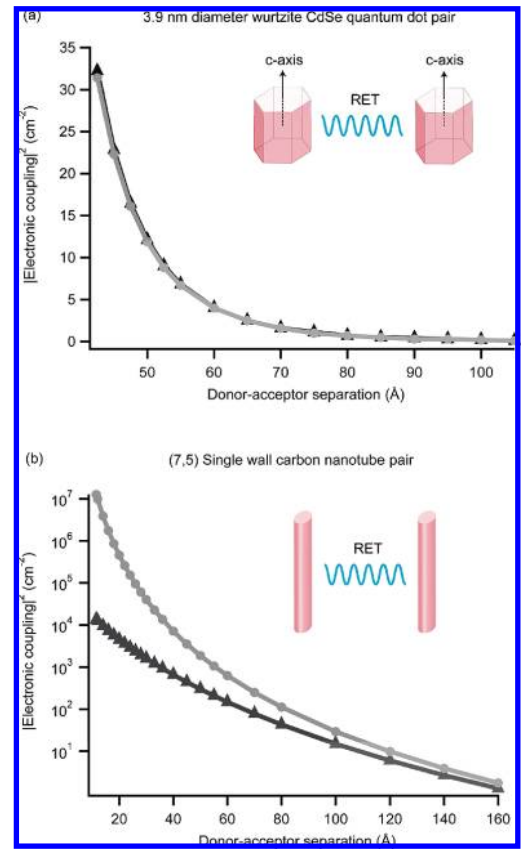

Figure 3. Squared electronic couplings predicted by the point-dipole model (circles) and by a multicentric transition density approach (triangles) as a function of the donor−acceptor center-to-center separation. (a) Two 3.9 nm diameter wurtzite CdSe quantum dots aligned parallel with respect to their crystallographic *c*-axis. (b) Two parallel (7,5) semiconducting single wall carbon nanotubes.

orbitals on an intervening molecular scaffold. Closs and co-workers first realized how to test the significance of a through-bond pathway for electronic coupling by noting the qualitative relationship between triplet−triplet RET and a concerted electron and hole transfer.[43] By using the structural rules governing electron transfer through σ-bond bridges,[44−48] it could be shown that the part of the electronic coupling that depends explicitly on donor−acceptor orbital overlap can effect RET between remote chromophores by operating through-bond. The interchromophore orbital overlap dependent interactions are solely responsible for triplet−triplet RET but act in concert with the Coulombic interaction that has already been described, for the case of singlet−singlet RET.[49] Since this early work on through-bond interactions, a number of studies have explored the role of various molecular bridges in transmitting electronic coupling for RET, as summarized previously in ref 2. More recently, a series of papers by Albinsson and co-workers have provided considerable insights into the nature of triplet−triplet through-bond RET.[50−52]

4.1. Through-Bond Interactions and Orbital Overlap. To consider interchromophore orbital overlap-dependent interactions, the exciton basis set used for calculations needs to be expanded using charge transfer (CT) configurations. For the sake of simplicity, let us consider a bichromophoric donor−acceptor system, where the full basis set now includes localized excitations on the two chromophores ($|D^*A\rangle$ and $|DA^*\rangle$) and the charge transfer configurations among them ($|D^+A^-\rangle$ and $|D^-A^+\rangle$). As described by Scholes et al.[53] and Thompson et al.,[54] these electronic configurations mix together in the bichro-

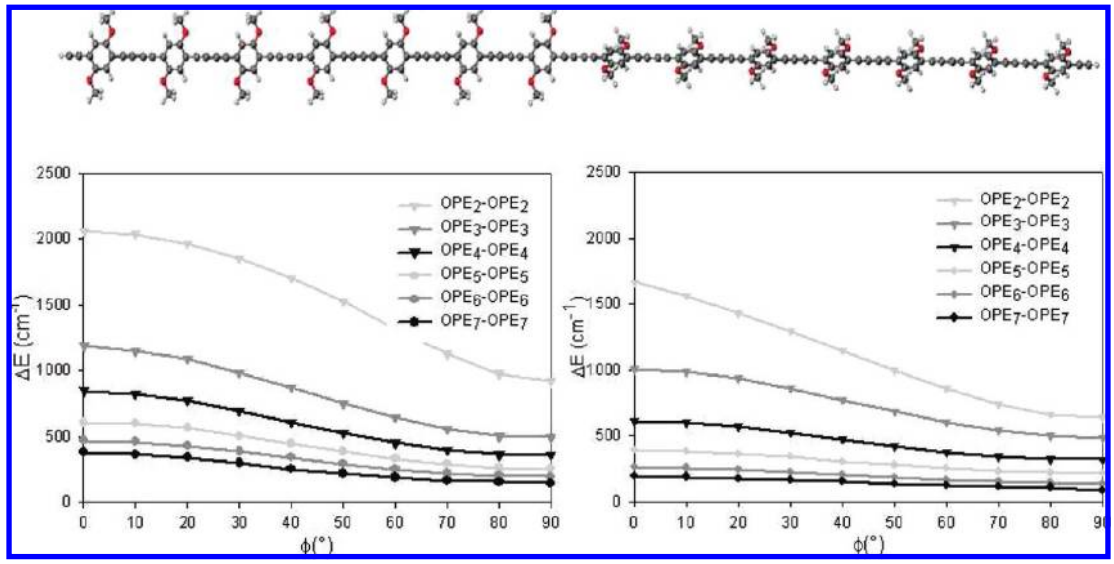

Figure 4. Evolution of the excited-state splitting, ΔE, with torsion angle, ϕ, in bichromophoric systems comprised of two oligophenylenebutadiynylenes of varying lengths separated by a conformational kink: (left) ground-state geometry; (right) transition-state geometry.

mophore via either purely covalent $\langle D^*A|H_{DA}|DA^*\rangle$, ionic, e.g. $\langle D^+A^-|H_{DA}|D^-A^+\rangle$, or mixed-type (e.g., $\langle D^*A|H_{DA}|D^-A^+\rangle$) interactions. These couplings can be partitioned into a long-range Coulomb contribution, that is operative provided spin selection rules are obeyed, and short-range contributions that invoke direct overlap between the wave functions of the two chromophores. The latter encompass two-electron exchange terms and one-electron transfer integrals that both decay exponentially with distance.[49] The Förster rate is obtained by developing solely the covalent electronic matrix element, $\langle D^*A|H_{DA}|DA^*\rangle$, in a multipolar expansion around the molecular centers and retaining only the lowest-order dipole contribution.

In covalently linked donor−acceptor dyads, the mixing between covalent and ionic configurations can be driven by through-bond interactions, mediated mostly by one-electron resonance integrals (the Hückel β integrals). A simple calculation allowing disentangling of through-bond from through-space contributions to the electronic coupling in symmetric bichromophoric model systems is to follow the energy splitting, ΔE, between the lowest two adiabatic electronic excited states (eigenfunctions of $H = H_D + H_A + H_{DA}$) as a function of the dihedral angle, ϕ, between the two chromophores (note that in this case D ≡ A and the electronic coupling is $\Delta E/2$).[55,56] This is shown in Figure 4a for two oligophenylenebutadiynylenes of varying lengths separated by a conformational kink. Because of the rotational symmetry around the main molecular axis (the transition dipoles on the two chromophores are coaligned along the rod direction), a completely flat dependence of ΔE on ϕ is expected if only through-space interactions would be operative. The full calculations, however, show a much more pronounced increase in the splitting as the dihedral angle is reduced. This arises from through-bond interactions between the two conformational subunits and simply reflects changes in π-delocalization.

It is interesting to note that the overall excited-state splitting decreases with increasing oligomer size, an evolution that reflects the dilution of the excited-state wave function over the subunits and the concomitant lower amplitude contributions at the edges of the interacting chromophores. As a result, both the long-range Coulomb interactions and the transfer integrals that contribute, respectively, to the though-space and through-bond couplings lessen with the number of repeating units.

It is also instructive to consider how the overall picture is affected when considering geometric relaxation phenomena in the excited state, i.e., in the limiting case of incoherent transport where the system is thermally equilibrated in the excited-state geometric configuration of the donor before hopping to the acceptor. The D−A electronic coupling is usually calculated on the basis of the geometry of the reactants (the donor in its excited-state geometry and the acceptor in its ground-state geometry) rather than at the transition state between reactants and products (where the electronic excitation spreads symmetrically over the donor and the acceptor), thus invoking the Franck−Condon approximation. However, in view of the high sensitivity of the electronic interactions with geometric structure, this approximation is questionable and we have therefore computed the couplings at the transition-state geometry.

The results reported in Figure 4b reveal a weaker dependence of ΔE with ϕ compared to the ground-state calculations in Figure 4a. This arises because of the self-localization induced by geometric relaxation phenomena and the resulting smaller end-chain contributions to the excited-state wave functions, and therefore smaller through-bond interactions. The effect is especially pronounced for the longest conjugated segments, for which a very flat dependence of ΔE with respect to ϕ is found. We have set up a simple four-state model, including the four electronic configurations described above, that is parametrized on the basis of a quantum-chemical description of the electronic excited states.[55] The model provides for a direct relationship between the through-bond contribution to the electronic coupling and the amount of charge transfer character in the lowest adiabatic electronic states and successfully accounts for the effect of geometric relaxation; see ref 55 for details.

4.2. Through-Bond Interactions and Coulombic Coupling. Recent single molecule spectroscopic studies have revealed a "non-Förster" behavior in a molecular triad, with a departure from the expected linear dependence between the measured energy transfer rates and spectral overlaps.[57] Such a deviation is particularly surprising, as the linear absorption of the donor−bridge−acceptor molecule, whose chemical structure is shown in Scheme 1, is almost exactly identical to the superimposed spectra of the individual subunits. However, from a detailed *ab initio* quantum-chemical investigation, we found that the electronic excitations, mostly confined on the (perylenedi-

SCHEME 1: Structure of the Bridged Perylenediimide (PDI) and Terrylenediimide (TDI) Bichromophore

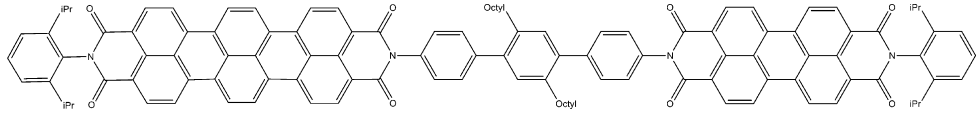

imide, PDI) donor and (terrylenediimide, TDI) acceptor, do slightly spread over the terphenyl spacer (though not enough to yield a measurable shift in the absorption/emission spectrum).[58] Thus, through-bond interactions lead to a slight delocalization of the transition densities over the spacer, which results in a net increase in the coupling between the "effective" donor and acceptor. That is, the Coulombic interaction is perturbed by the intervening bridge. This is further confirmed by the high sensitivity of the calculated electronic interaction on the partitioning scheme. Namely, the inclusion of one, two, or three phenylene units in the effective donor (or acceptor) leads to large changes in couplings (by up to 56%). The breakdown of the point-dipole approximation and Förster model in this case thus mostly arises from an effective interchromophoric distance between the interacting chromophores that is significantly smaller than the center-to-center separation between the PDI and TDI cores.

5. Coherence, Correlations, and Spectral Overlap

In the original derivation of the formula for resonance energy transfer, Förster made a number of assumptions, all of which were sensible for the experiments he was attempting to understand. Among those assumptions were that the environments of the donor and acceptor are independent of one another and that the donor and acceptor are single molecules far from one another so that there is no coherent interaction between them. Recent experiments in which the donor and acceptor are close enough to question these FRET assumptions have led to a renewed interest in these issues.[59−61] Memory effects and the intermediate coupling regime of CRET are thus starting to attract considerable attention.

5.1. Molecular Aggregates as Donors and Acceptors (GFT). To begin with, consider a multichromophoric aggregate acting as a donor or acceptor; that is, the donor and/or acceptor are made up of a number of coherently (strongly) coupled molecules, Figure 5a. The excited states of the *effective* donor and/or acceptor are then linear combinations of the excited states of the individual molecules—a collection of molecular exciton states. Does the standard FRET formula hold in this case? It is easy to see that, in general, it may not. Consider a situation in which the donor consists of a pair of identical molecules situated a distance d apart along the x-axis (Figure 5b) and assume that the transition dipole points along the y-axis. The interaction matrix element V between the two donor molecules is then positive and the two-exciton states that are formed are

$$|\pm\rangle = (\phi_1 \pm \phi_2)/\sqrt{2} \tag{3}$$

Here, ϕ_1 (ϕ_2) refers to the product state with molecule 1 (2) excited and the other molecule in the ground state. Because the interaction matrix element is positive in this cofacial H-aggregate, then $|-\rangle$ has lower energy than $|+\rangle$. Note that $|-\rangle$ also has a vanishing transition dipole moment, $\vec{\mu}_- = (\vec{\mu}_1 - \vec{\mu}_2)/\sqrt{2} = 0$, and according to the standard Förster result, there can therefore be no FRET from this state to an acceptor (or *vice versa*). However, the matrix element for energy transfer is actually given by

$$\langle -;A_g|V_{dd}|D_g;A_e\rangle = (\langle \phi_1;A_g|V_{dd}|D_g;A_e\rangle - \langle \phi_2;A_g|V_{dd}|D_g;A_e\rangle)/\sqrt{2} \tag{4}$$

where A_g is the acceptor ground state, A_e is its excited state, and D_g is the aggregate donor ground state. Since the distance between the acceptor A and molecule 1 is different than the distance between molecule 2 and A, this matrix element does not vanish, so energy transfer is possible from the dark state. In the limit that A is very far from the donor pair, the matrix element becomes small, so the Förster formula applies. Some examples along these lines are given in Table 1 of ref 2.[62]

A number of authors have derived the general formula for the energy transfer rate in the case of multichromophoric donors and acceptors.[63−65] The theory required in this simple case where the system is partitioned into strong and weak coupling parts is called generalized förster theory (GFT). Various approximations to the general formula lead to slightly different results, but the main point is clear: the standard Förster result cannot in general be used for multichromophoric donors and/or acceptors.

This principle has, for example, enabled explanation of the observed RET rates in the reaction center of purple bacteria.[66] Using the special pair of the reaction center as an example, Figure 5c, it is obvious that P_+ is a dark state (the transition density is symmetric and therefore dipole-forbidden), whereas

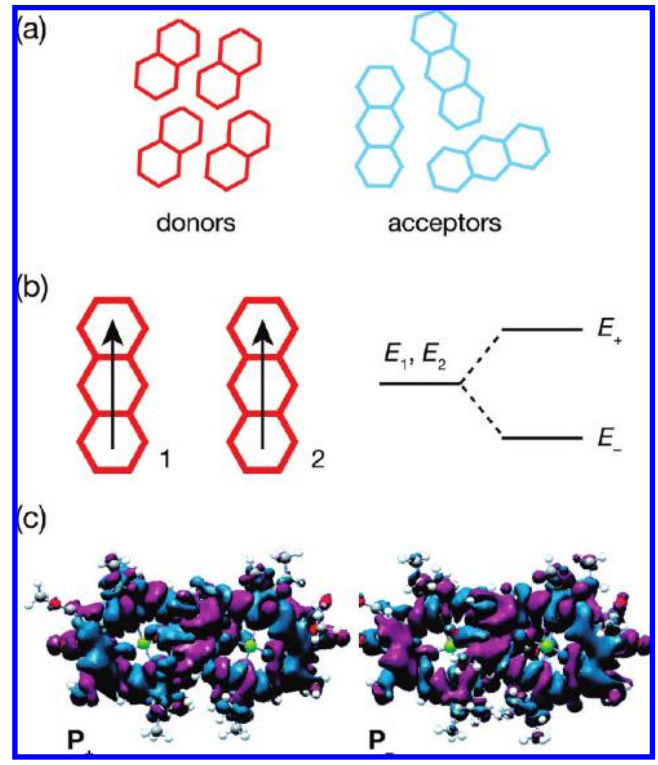

Figure 5. (a) Illustration of an aggregate donor−acceptor system. Strong coupling within each of the donor and acceptor groups forms molecular exciton states that are the effective donor and acceptor states in GFT. (b) Depiction of the model dimer system discussed in the text. (c) Transition densities calculated for the upper P_+ and lower P_- exciton states of the special pair dimer in the photosynthetic reaction center of the purple bacterium *Rhodobacter sphaeroides*.

the P_- state is bright. The labeling of P_+ and P_- differs from the model system described above because the interaction matrix element in the special pair dimer is negative owing to the particular orientation of the bacteriochlorophylls. In contrast to the prediction of FRET theory, both P_+ and P_- turn out to be equally effective acceptor states. The explanation, from the transition density point of view, is that the bacteriochlorophyll donor positioned on one side of the special pair "sees" predominantly only one side of the dimer transition density, which looks the same whether the acceptor is P_+ or P_-.

5.2. Spectral Overlap and the Structure of the Bath. Recent experiments have suggested that the coherent interaction between donor and acceptor may be large enough to lead to oscillatory terms in the RET rate, and this has stimulated interest in understanding the manifestation and implications of intermediate coupling. We consider here some of the subtleties involved in this limit, showing why understanding the bath of nuclear degrees of freedom may in fact be central to gaining a deeper understanding of quantum coherent energy transport.

Let us examine the assumption of independent environments, that is, the collection of modes (of the molecules or the solvent) that interact with the donor and acceptor. This assumption is crucial to the result that the rate of energy transfer is proportional to the overlap of the donor emission and the acceptor absorption. It is clear that if D and A are close, there may be modes that interact with both, and this changes that proportionality. To see how this situation might affect RET theory, consider a mode that is coupled strongly to both D and A but in exactly the same manner. This mode will clearly show up in the donor emission and the acceptor absorption but cannot participate in the transfer process, since the matrix element for transfer will be zero unless that mode does not change its state in the transfer.

We model the environments of donor and acceptor by a collection of harmonic modes, with the donor (acceptor) excited state linearly coupled to mode λ with a coupling constant g_λ^{D} (g_λ^{A}). Each of these exciton−phonon coupling constants is proportional to the displacement along vibrational mode λ of the donor (acceptor) excited state with respect to the ground-state geometry, and $(g_\lambda^{\mathrm{D}})^2\hbar\omega_\lambda$ ($(g_\lambda^{\mathrm{A}})^2\hbar\omega_\lambda$) is the corresponding reorganization energy. Then, the Fermi golden rule rate of RET between donor and acceptor yields

$$k_{\mathrm{DA}} = \frac{|V_{\mathrm{DA}}|^2}{h}\mathrm{Re}\int_{-\infty}^{+\infty} \mathrm{d}t\, \exp(i\omega_{\mathrm{DA}}^{0-0}t) \times \exp\left[-\sum_\lambda (g_\lambda^{\mathrm{D}} - g_\lambda^{\mathrm{A}})^2(2\bar{n}(\omega_\lambda) + 1)\right] \times \exp\left[\sum_\lambda (g_\lambda^{\mathrm{D}} - g_\lambda^{\mathrm{A}})^2\{\bar{n}(\omega_\lambda)\exp(i\omega_\lambda t) + (\bar{n}(\omega_\lambda) + 1) \times \exp(-i\omega_\lambda t)\}\right] \quad (5)$$

Here, $\omega_{\mathrm{DA}}^{0-0}$ denotes the energy gap between the donor and acceptor adiabatic transitions; $\bar{n}(\omega_\lambda) = [\exp(\omega_\lambda/k_{\mathrm{B}}T) - 1]^{-1}$ is the temperature-dependent occupation number of vibrational state λ. From eq 5, it is clear that, if $g_\lambda^{\mathrm{D}} = g_\lambda^{\mathrm{A}}$, then the contribution of that mode to the rate vanishes, even though it participates in the absorption and emission processes (e.g., it contributes to line broadening).

If we choose to make the assumption that the nuclear modes are independent, meaning that, for each λ, either g_λ^{D} or g_λ^{A} is zero, eq 5 can be factorized into a product of donor ($\tilde{F}_{\mathrm{D}}$) and acceptor ($\tilde{F}_{\mathrm{A}}$) line shapes, resulting in the FRET rate:

$$k_{\mathrm{DA}} = \frac{1}{\hbar^2}|V_{\mathrm{DA}}|^2\mathrm{Re}\int_{-\infty}^{+\infty}\mathrm{d}\omega_\lambda \tilde{F}_{\mathrm{A}}(\omega_{\mathrm{DA}}^{0-0} - \omega_\lambda)\tilde{F}_{\mathrm{D}}(\omega_\lambda) = \frac{1}{\hbar^2}|V_{\mathrm{DA}}|^2 J \quad (6)$$

where $J = \mathrm{Re}\int_{-\infty}^{+\infty}\mathrm{d}t\,\exp(i\omega_{\mathrm{DA}}^{0-0}t)f_{\mathrm{A}}(t)f_{\mathrm{D}}(t)$ is the Förster overlap factor obtained by convolution of the acceptor and donor response functions, defined similarly to that in eq 1b.

In the general (non-Förster) case, both local and nonlocal (i.e., shared) modes are coupled to the electronic excitations, then it is clear that the rate expression will not factor into separate functions for A and D. In this case, the convolution theorem leads to a double convolution product expression for the overlap function:

$$J_{\mathrm{NF}} = \mathrm{Re}\int_{-\infty}^{+\infty}\mathrm{d}t\,\exp(i\omega_{\mathrm{DA}}^{0-0}t)f_{\mathrm{A}}(t)f_{\mathrm{D}}(t)f_{\mathrm{DA}}(t) = \frac{1}{\sqrt{2\pi}}\mathrm{Re}\int_{-\infty}^{+\infty}\mathrm{d}\omega_1\int_{-\infty}^{+\infty}\mathrm{d}\omega_2\tilde{F}_{\mathrm{A}}(\omega_{\mathrm{DA}}^{0-0} - \omega_1)\tilde{F}_{\mathrm{D}}(\omega_{\mathrm{DA}}^{0-0} - \omega_2)\tilde{F}_{\mathrm{DA}}(\omega') \quad (7)$$

where the renormalization function $\tilde{F}_{\mathrm{DA}}(\omega')$ involves those modes, with frequencies $\omega' \in \{\{\omega_1\} \cap \{\omega_2\}\}$ that are simultaneously coupled to D and A. This term alters the spectral overlap from the FRET overlap factor J.

The development leading to eq 7 shows how bath memory effects can play a role in mediating coherent energy transport, even in the weak coupling limit. The bath now retains memory of the donor state after transfer of excitation to the acceptor, which in turn can contribute oscillations to the transfer probability. The result of eq 7 reduces to the Förster expression when the shared modes are treated as Markovian and very quickly relaxing, in which case $f_{\mathrm{DA}}(t) = 1$.

In the limiting case that $g_\lambda^{\mathrm{D}} \neq g_\lambda^{\mathrm{A}}$ in eq 5, and both are nonzero, the energy transfer process along that coordinate looks more like the Marcus model for electron transfer[67] rather than the standard Förster model for energy transfer. That is because the spectral overlap contains only common modes for the donor and acceptor, but the coupling to them changes during the transition form reactant to product state. Hence, it is a fluctuation that is shared by donor and acceptor that enables the transition; essentially, this is a case of implicit correlation of fluctuations along the reaction coordinate.

Numerical simulations can be performed by expanding eq 7 into mode specific terms, or, instead, by considering the linear displaced Brownian harmonic oscillator model where the complete set of normal modes is partitioned into a set of primary modes linearly coupled to the electronic transitions that in turn couple to a set of harmonic oscillators characterized by their spectral densities.

We performed numerical simulations of the spectral overlap, including the possibility that a single mode is shared according to eq 7. As a model donor−acceptor system, we use the two lowest energy bilin chromophores of phycocyanin 645 (PC645) antenna from the cryptophyte algae *Chroomonas CCMP270.* The donor and acceptor line shapes were taken to be a sum of two overdamped Brownian oscillators (BOs), representing the homogeneous line broadening, and a sum of discrete oscillators (DOs), describing intramolecular vibrations. We used transition energies of 1.94 and 1.93 eV for donor and acceptor, respec-

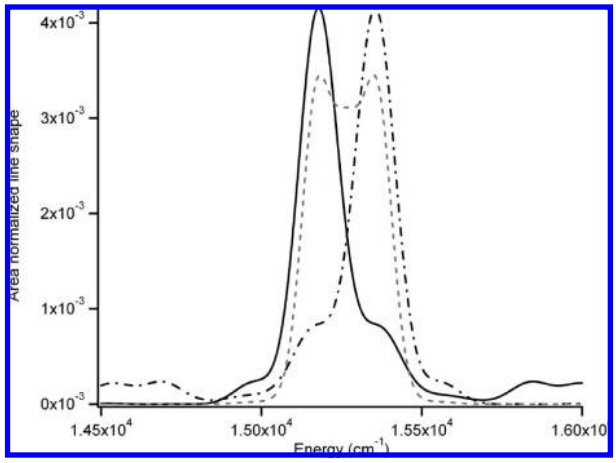

Figure 6. Spectral overlap (dashed line) of the area-normalized donor emission line shape (dash-dotted line) and area-normalized acceptor absorption line shape (solid line) for the two low energy bilins of phycocyanin 645 (PC645) from cryptophyte algae *Chroomonas CC-MP270.* Line shapes correspond to donor and acceptor transition energies of 1.94 and 1.92 eV, respectively (see text for details).

TABLE 2: Spectral Overlap Factors between the Two Low Energy Bilins of PC645 for Various Cases of Shared Modes[a]

	$\omega_A = 1.93$ eV		$\omega_A = 1.92$ eV		$\omega_A = 1.91$ eV	
shared mode[b]	J (10^{-3} cm)	% change	J (10^{-3} cm)	% change	J (10^{-3} cm)	% change
none	2.01		1.50		1.01	
BO 1	2.20	9	1.73	15	1.00	−1
BO 2	2.38	18	1.39	−7	0.995	−1
DO 1	2.73	36	1.18	−22	1.05	4
DO 2	2.77	38	2.51	67	1.12	11
DO 3	1.86	−8	2.20	47	1.55	53
DO 4	1.83	−9	2.14	43	1.50	49
DO 5	1.53	−24	2.19	46	1.70	68
DO 6	1.90	−6	1.97	32	1.33	32
DO 7	1.58	−21	2.14	43	1.61	59
DO 8	1.99	−1	1.80	20	1.19	18

[a] The various calculations used eq 7 and assume either independent nuclear modes or the possibility that one mode is shared between donor and acceptor with same sign displacements. The donor transition energy is 1.94 eV, while various acceptor transition energies are chosen to be 1.93, 1.92, and 1.91 eV. [b] Donor and acceptor line shape functions taken to be a sum of two overdamped Brownian oscillators (BOs), each with reorganization energy $\lambda = 130$ cm^{-1} and modulation frequencies $\Lambda_1 = 20$ and $\Lambda_2 = 0.67$ ps^{-1}, and a sum of discrete bath oscillators (DOs) with frequencies in cm^{-1} (Huang−Rhys factors): 10 (0.5), 200 (0.1), 665 (0.05), 818 (0.04), 1108 (0.04), 1270 (0.02), 1370 (0.03), and 1645 (0.01) (values estimated in ref 68). Discrete oscillators are numbered in order of increasing frequency.

tively, corresponding to the values estimated from ref 68. DO and BO line functions were calculated for $T = 298$ K according to eqs 8.39 and 8.49 of ref 69. In addition, we considered spectral overlaps for model cases where the transition energy of the acceptor is shifted to 1.92 and 1.91 eV. We did not include static disorder in these calculations.

In Figure 6, we show the standard spectral overlap obtained from the donor and acceptor line shapes, assuming no shared modes. In Table 2, we report spectral overlap factors calculated for various cases where we considered none or one single Brownian oscillator or the discrete oscillator mode to be shared between the donor and acceptor. For illustration, here, we only consider the case corresponding to same sign displacements for the shared mode. The results show how the absence of a shared mode in the FRET expression leads in most cases to net increases in the effective overlap, although in the same cases significant decreases are also found. In particular, intramolecular vibrations induce variations that can be very significant (∼70%), while environmental BO modes cause smaller changes (<20%). It is also interesting to analyze the impact of high and low frequency shared modes as the energy of the main peaks of the chromophores is shifted. When ω_A is 1.93 eV, the two peaks overlap very well, and increases of ∼10−40% are predicted for the overlap factor when a BO or a low frequency DO mode is shared. However, when ω_A is red-shifted to 1.92 or 1.91 eV, this effect progressively becomes negligible. On the contrary, the impact of sharing high frequency vibrations progressively increases as the overlap between the main peaks worsens. This behavior can be explained to be due to the more important role of the vibrational side peaks in the case of poor overlap compared to the situation in which the main peaks of D and A overlap very well.

In addition, we can derive an analytical expression for the RET rate in the case where a continuous distribution of low-frequency vibrational modes over the donor and acceptor leads to Gaussian line shapes. For spectral line shapes, this is known as the slow modulation limit of the Brownian oscillator model (in the high temperature limit).[69,70] We develop this model to illustrate a feature of the low frequency bath modes that contribute line broadening. The reader should note that the model does not account for the contribution of high frequency, intramolecular, modes to spectral overlap (vibronic progressions in the spectra), which are often quantitatively important for ensuring energy conservation. For independent Gaussian baths (GBs), the Förster overlap in eq 6 then becomes

$$J_{F-GB} = \sqrt{\frac{2\pi}{\sum_\lambda [(g_\lambda^D)^2 + (g_\lambda^A)^2]\omega_\lambda[2\bar{n}(\omega_\lambda) + 1]\omega_\lambda}} \times \exp\left[\frac{-\{\omega_{DA}^{0-0} - \sum_\lambda [(g_\lambda^D)^2 + (g_\lambda^A)^2]\omega_\lambda\}}{2\sum_\lambda [(g_\lambda^D)^2 + (g_\lambda^A)^2]\omega_\lambda[2\bar{n}(\omega_\lambda) + 1]\omega_\lambda}\right] \quad (8)$$

This expression is similar to the Marcus charge transfer rate expression in the semiclassical limit.[67] It is equivalent to the Förster rate in the Gaussian approximation. The spectral overlap (and therefore transfer rate) is maximized when the adiabatic donor−acceptor electronic gap is exactly compensated by the reorganization energy associated with the energy transfer process, which is simply the sum of the donor and acceptor relaxation energies: $\lambda_{reorg} = \sum_\lambda [(g_\lambda^D)^2 + (g_\lambda^A)^2]\ \hbar\omega_\lambda$. In the general case, the acceptor line shape must be convoluted with the effective donor emission line shape that itself results from the convolution between $\tilde{F}_D(\omega - \omega_1)$ and $\tilde{F}_{DA}(\omega_1)$. Applying the Gaussian approximation to eq 7 leads to an effective donor emission line shape that is shifted to larger (smaller) donor−acceptor transition energies for negative (positive) values of the cross terms $-2g_\lambda^D g_\lambda^A \omega_\lambda$. The spectral overlap takes the form of eq 8, where $[(g_\lambda^D)^2 + (g_\lambda^A)^2]\omega_\lambda$ is replaced by $[(g_\lambda^D)^2 + (g_\lambda^A)^2 - 2g_\lambda^D g_\lambda^A]\omega_\lambda$ (i.e., after renormalization of the reorganization energy by the cross product):

$$J_{\mathrm{NF-GB}} = \sqrt{\frac{2\pi}{\sum_{\lambda}[(g_{\lambda}^{\mathrm{D}} - g_{\lambda}^{\mathrm{A}})^2]\omega_{\lambda}[2\bar{n}(\omega_{\lambda}) + 1]\omega_{\lambda}}} \times \exp\left[\frac{-\{\omega_{\mathrm{DA}}^{0-0} - \sum_{\lambda}[(g_{\lambda}^{\mathrm{D}} - g_{\lambda}^{\mathrm{A}})^2]\omega_{\lambda}\}}{2\sum_{\lambda}[(g_{\lambda}^{\mathrm{D}} - g_{\lambda}^{\mathrm{A}})^2]\omega_{\lambda}[2\bar{n}(\omega_{\lambda}) + 1]\omega_{\lambda}}\right] \quad (9)$$

In the Gaussian model, the donor and acceptor free energy surfaces are represented by the usual parabolas. For a single discrete vibrational mode λ, it is clear that, in comparison to the Förster limit, the reorganization energy for RET is reduced in the case of displacements with the same sign and increased in the case of displacements of opposite sign.

This section has shown how important it is to consider *details* of the bath, including its characteristic frequencies and how they couple to the donor and acceptor transitions. Thus, elucidating details of the bath of nuclear motions coupled to the donor and acceptor transitions, especially the length scale of bath fluctuations, are important challenges for future work. Researchers need to be aware that the Bloch-type dephasing models, which reduce $f_{\mathrm{D}}(t)$ and $f_{\mathrm{A}}(t)$ to Lorentzian line shapes, correspond to the infinite temperature limit and do not provide sufficient information about the nature of the bath to yield useful insights about coherent energy transfer phenomena in molecular systems.

5.3. Intermediate Coupling and Coherent Dynamics. The intermediate regime for RET can be put into perspective by considering the limiting cases. In the case of weak electronic coupling (V) between the chromophores, the excitation is localized on a chromophore. That is perceived as the Stokes shift happening only at one site, yielding the thermodynamic equilibrium nuclear configuration of a single chromophore in its excited state.[71−73] Excitation may then be transferred among chromophores in a multichromophoric assembly by FRET in the manner of a classical random walk. These incoherent hops are caused by the interchromophore electronic coupling, which thus acts as the perturbation promoting the transition. In the strong coupling case, molecular exciton states are formed as coherent superpositions of the various ways that excitation can be placed among the sites. In this limit, excitation can diffuse over long distances, such as in a crystal, in a wavelike manner.[74−77] In a confined system, like a molecular aggregate, excitation cascades down a ladder of eigenstates, instigated by perturbative coupling to the bath.[78−80]

Traditionally, the conditions for strong coupling are that we have $h/V \ll \tau_{\mathrm{decoh}}$, while for weak coupling $h/V \gg \tau_{\mathrm{decoh}}$,[71] where h is Planck's constant and V signifies the expectation value of the electronic coupling between molecules. Then, h/V is the electronic coupling period, and τ_{decoh} is the decoherence time of the excited state. The intermediate coupling case lies in between, such that $h/V \sim \tau_{\mathrm{decoh}}$. A difficulty in dealing with this case is that the electronic coupling and the exciton-bath coupling need to be treated on equal footing; we cannot trace one out of the dynamics problem.

The time-dependent population density of the electronically excited acceptor state, $|\mathrm{a}\rangle$, $\rho_{\mathrm{a}}(t) = c_{\mathrm{a}}^{*}(t)c_{\mathrm{a}}(t)|\mathrm{a}\rangle\langle\mathrm{a}|$, evolves after initial preparation of $|\mathrm{d}\rangle$ according to[81]

$$\rho_{\mathrm{a}}(t) = \mathrm{Tr}[\langle \mathrm{d}|V_{+}(t')|\mathrm{a}\rangle\langle\mathrm{a}|V_{-}(t')|\mathrm{d}\rangle\rho_{\mathrm{d}}] \quad (10)$$

where $\mathrm{Tr}[\rho_{\mathrm{d}}...]$ means a thermal average is taken over the population of the initial states. Time goes right to left. The time-dependent operators are written in terms of time-ordered operators:

$$V_{\pm}(t') \equiv \exp_{T}\left\{\pm\frac{i}{\hbar}\int_{0}^{t'} H(t')\,\mathrm{d}t'\right\} \quad (11)$$

where the Hamiltonian H contains both the electronic coupling V as well as the fluctuating exciton-bath coupling. Equation 10 contains some features that are important for understanding CRET. First, we need to be able to treat both the electronic coupling and the bath fluctuations that are strongly coupled to the electronic transitions nonperturbatively. It has been found that this can be achieved using a unitary transformation of the Hamiltonian, often known as the small polaron transformation.[81−83] Second, we need to permit the propagation of populations as well as coherent superposition states (coherence transfer). Coherence transfer is neglected by making the secular approximation in master equation formulations.[8]

The intuition that can be gained by inspection of eq 10 is that the evolution of the probability density is determined by a forward ($|\mathrm{d}\rangle$ to $|\mathrm{a}\rangle$) and reverse propagation of the system. Throughout each of these paths, the states $|\mathrm{d}\rangle$ and $|\mathrm{a}\rangle$ can couple directly to each other via V, or they can interact with the bath degrees of freedom, causing energy fluctuation at the sites. In the FRET limit, there are so many nuclear fluctuations sampled during any trajectory that the forward path is completely different than the reverse path, so memory is lost. The excitation is thus equilibrated and localized before and after RET through a site energy renormalization caused by strong phonon "clothing" of the excitation at each site[82] (a lattice relaxation with the same origin as the Stokes shift). In the strong coupling limit, the electronic coupling drives the system from donor to acceptor site at a frequency much faster than the bath equilibration time, thus preserving phase memory and forming delocalized stationary states, like those written in eq 3. In the intermediate coupling case, site energies and intersite couplings are renormalized by phonon clothing and energy moves in a way that retains some phase memory. That leads to electronic oscillations of the kind that have recently been observed in experimental data.[60]

Using a simplistic Markovian, infinite temperature bath model, so that the site transition energy fluctuations are uncorrelated and described by the delta function correlation function with a decoherence time of τ_{decoh}, eq 10 can be solved, but the result has been found to predict incorrectly that the populations on each site are always equal at infinite time.[81] That problem is related to the infinite temperature bath model and can be resolved by more elaborate models. Kakitani and coworkers have provided a simple solution that illustrates the difference between weak, intermediate, and strong coupling regimes for a homodimer,[85] Figure 7. In the weak coupling limit, the acceptor population density increases exponentially with time, meaning that we can define a rate constant for RET. That convenient relationship breaks down in the intermediate coupling regime, where coherent oscillations of population between donor and acceptor may even be observed. These oscillations mean that there is a phase relationship between donor and acceptor sites at the amplitude level, which leads to quantum coherent dynamics. Coherent electronic oscillations also mean that the bath cannot equilibrate, and it therefore contributes memory effects to the dynamics.[86] In the long time limit, each plot tends to 0.5, irrespective of whether the dynamics occur in the weak or strong coupling limits.

5.4. Contributions and Prospects of Experiment. Theorists have contemplated the possibility of memory effects and

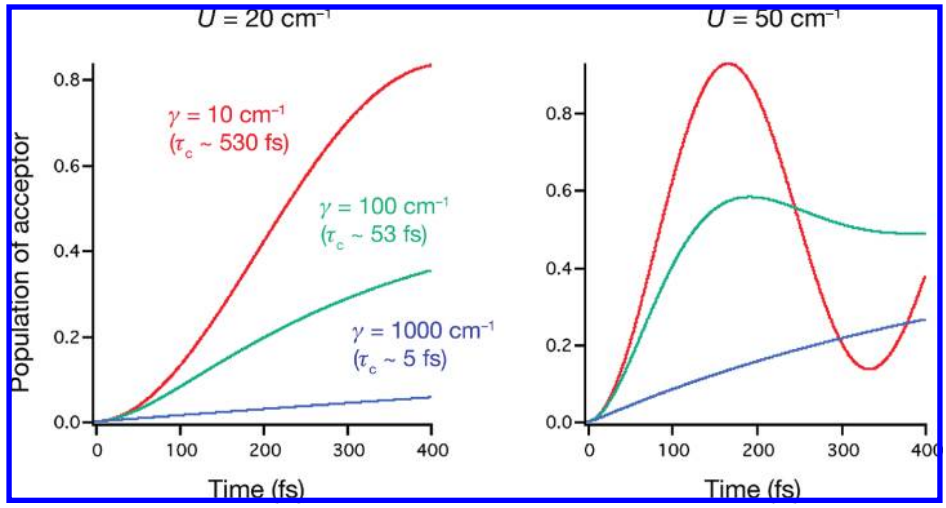

Figure 7. Calculations of the evolution of acceptor population density as a function of time after photoexcitation of the donor, based on eqs 29 and 30 of ref 84. U is the electronic coupling between donor and acceptor. The line width parameter is related to the decoherence time via $\gamma = \hbar/\tau_c$. An exponential relationship between acceptor population and time indicates the validity of the Fermi golden rule expression for RET. At long time, all the curves tend to 0.5.

coherent dynamics in energy transfer for some time, but progress was subdued because there were no compelling experimental demonstrations of such phenomena. Typically, the kinds of experiments that measure ultrafast energy transfer dynamics are pump−probe techniques. These techniques pump excited-state populations and probe the evolution of these population densities at various time delays, using a probe pulse.[69,87] Kinetic models tend to assert exponential population evolution, which precludes the observation of signatures of coherence. However, more fundamentally, it is because these kinds of experimental techniques prepare and probe populations that they are intrinsically unable to yield compelling evidence for coherence or memory effects. For example, ultrafast pump−probe spectroscopic data can show oscillations in signal intensity as a function of time—quantum beats. However, it is difficult to differentiate oscillations caused by coherent excitation of vibrations from those signaling coherent electronic population dynamics, like those plotted in Figure 7.

An important breakthrough was the realization that two-dimensional electronic spectroscopy,[88−90] specifically two-dimensional photon echo (2DPE) measurements, can discriminate between nuclear quantum beats and electronic coherent oscillations.[60,91] The underlying reason for that ability is that the data contain information about electronic coherences as well as populations. More significantly, the usual representation of the data correlates the frequency distribution characterizing the initial electronic coherence (ω_τ) with the coherence associated with the third-order nonlinear polarization (ω_t) radiated after the system has evolved (e.g., after RET) for a population time T.

At one level, the experiment allows us to associate donor state transition frequencies with acceptor state frequencies, thus permitting elucidation of RET pathways in addition to rates. In that case, cross-peaks are found to grow in with time.[92] Their position tells us that a donor chromophore with frequency $\omega_\tau = \omega_d$ transfers energy to an acceptor chromophore with energy $\omega_t = \omega_a$. Some compelling examples of this idea have been reported by the Fleming group.[93,94]

More detailed analysis of the data can, in some instances, reveal evidence for electronic coherences. These can be found in off-diagonal features, if they can be clearly resolved in the data, but can also be discerned in the main diagonal feature.[91,95,96] An example is shown in Figure 8. The intensity of the main peak in the 2D data is found to oscillate with population time, and that alone is similar to trends found in transient grating or pump−probe spectroscopy. However, the 2DPE data can correlate those intensity oscillations with changes in the peak shape. Electronic coherent oscillations tend to exhibit an anticorrelation of the peak intensity with its degree of "roundness", Figure 8. Physically, the underlying reason for that is that, in the case of nuclear quantum beats, the signal intensity is simply modulated by, for example, oscillating Franck−Condon factors as the nuclear wavepackets propagate. On the other hand, the electronic oscillations are caused by population density interconverting with electronic coherences. The 2D experiment can probe these coherences via their subtle off-diagonal signatures in the frequency−frequency correlation.

6. Solvent Screening

Solvent effects play a central role in the control of RET dynamics, not only because they cause line broadening, as discussed in the previous section, but also because they strongly screen the electronic interaction promoting RET. This was recognized early, in Förster theory, where the interaction between donor and acceptor transition dipoles is assumed to be modified through a simple screening factor $s = 1/n^2$, where n is the refractive index of the medium. The screening effect can be significant, yielding an ~4-fold reduction of the FRET rate in typical solvents. More sophisticated descriptions of solvent screening modify the Förster screening factor additionally through the square of a local field factor.[97,98]

Recent theoretical developments have allowed examination of the screening of the electronic coupling with an unprecedented level of detail. The influence of shape, distance, and mutual orientation between molecules on solvent screening turns out to be important at close donor−acceptor separations. Hsu and co-workers[99] showed, for example, that when the donor and the acceptor are closely spaced, so that they share a common cavity inside the dielectric environment, solvent effects can either reduce or enhance the overall interaction depending on the particular orientation between the chromophores. However, this study neglected the shape of the molecules by assuming spherical cavities, and that seems to have a significant effect

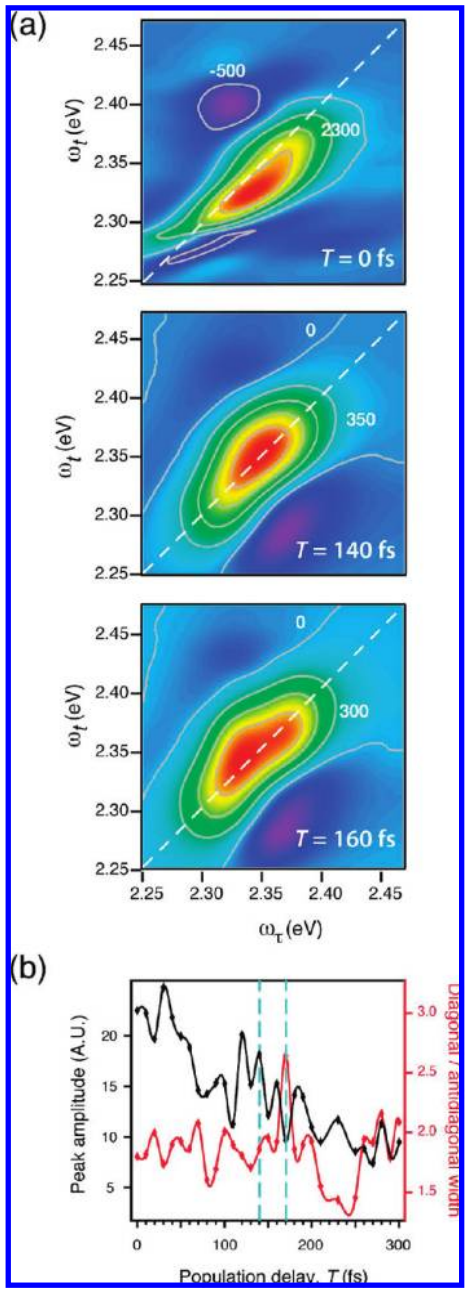

Figure 8. (a) 2DPE data for the conjugated polymer MEH−PPV in dilute solution (chloroform, 293 K) for three population times.[61] The evolution of intensity and shape of the main diagonal feature as a function of T provides the signature of electronic coherence. (b) A plot showing the anticorrelation in peak intensity versus diagonal/antidiagonal width at $1/e$ of the peak height as a function of population time. The anticorrelations at two population times are emphasized by the dashed vertical lines.

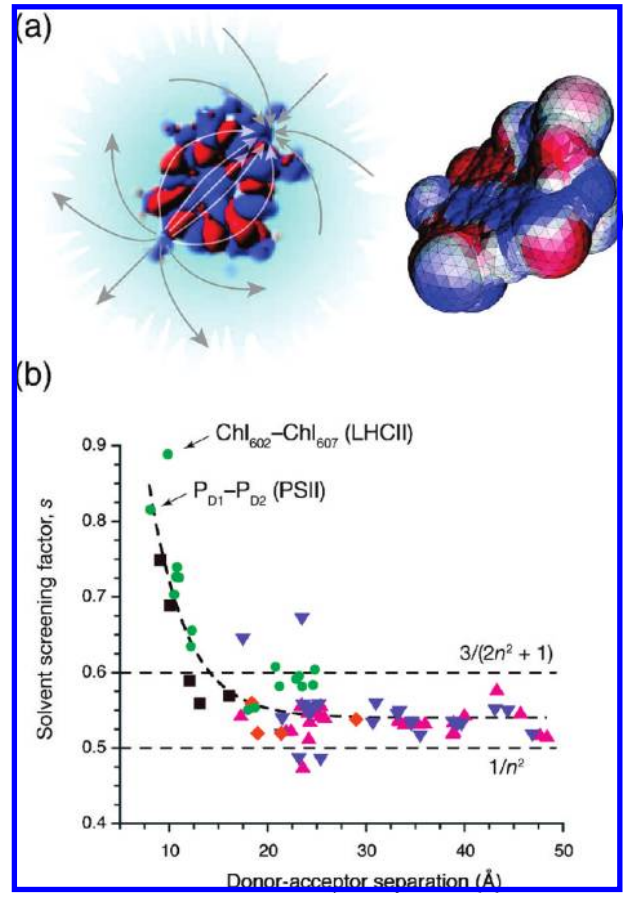

Figure 9. (a) The molecule's transition density (that of chlorophyll-*a* is plotted) polarizes the surrounding solvent through the interaction with the electric field indicated. This three-dimensional polarization can be represented as effective solvent charges collected on a surface enclosing the molecules, plotted on the right-hand side. (b) Solvent screening factors, s, predicted for various chromophore pairs of light-harvesting antennae proteins. The correspondence between data point and structure is pink triangles = PE545, blue squares = PC645, green circles = PSII or LHCII, except orange diamonds = data involving the carotenoid in PSII. The Förster value, $1/n^2$, is indicated by the lower horizontal line, and the Onsager value, $3/(2n^2 + 1)$, is the upper line. The dashed curve is a fit through the data points by eq 12. Reprinted from ref 103 with permission. Copyright 2007 American Chemical Society.

on the results. In recent work, more sophisticated models have been developed, in which the solvent response is calculated by solving the Poisson equation in realistic molecular-shaped cavities inside the dielectric medium.[100,101] As we describe below, this progress has enabled us to uncover a strong distance dependence of the solvent screening, which even modifies the traditional R^{-6} distance dependence of the FRET rate.

Let us first clarify the way solvent (in general, any host medium) modifies the electronic coupling promoting RET. First, solvation typically leads to an enhancement of the dipolar strength of electronic transitions. The corresponding *implicit* solvent effect on the coupling can be accounted for in Förster theory through the spectral overlap factor by considering spectra of the chromophores measured in the appropriate medium.[102] Second, an additional *explicit* solvent effect arises because the oscillating transition of the donor induces an oscillating polarization in the solvent, which, in turn, interacts with the acceptor (and *vice versa*).[99] That is illustrated schematically in Figure 9a. This solvent-mediated contribution leads in most cases to an overall reduction or *screening* of the donor−acceptor interaction, and is the focus of this section.

We have recently applied a novel quantum-mechanical approach to examine the solvent screening for a set of over 100 pairs of chromophores (chlorophylls, carotenoids, bilins) taken from structural models of photosynthetic light-harvesting antenna systems.[103,104] We found a striking exponential attenuation of the solvent screening at separations less than about 20 Å, thus interpolating between the limits of no apparent screening and a significant attenuation of the RET rate. This result reveals a previously unidentified contribution to the distance dependence of the RET rate, which indicates that Förster theory substantially underestimates RET rates at close donor−acceptor separations.

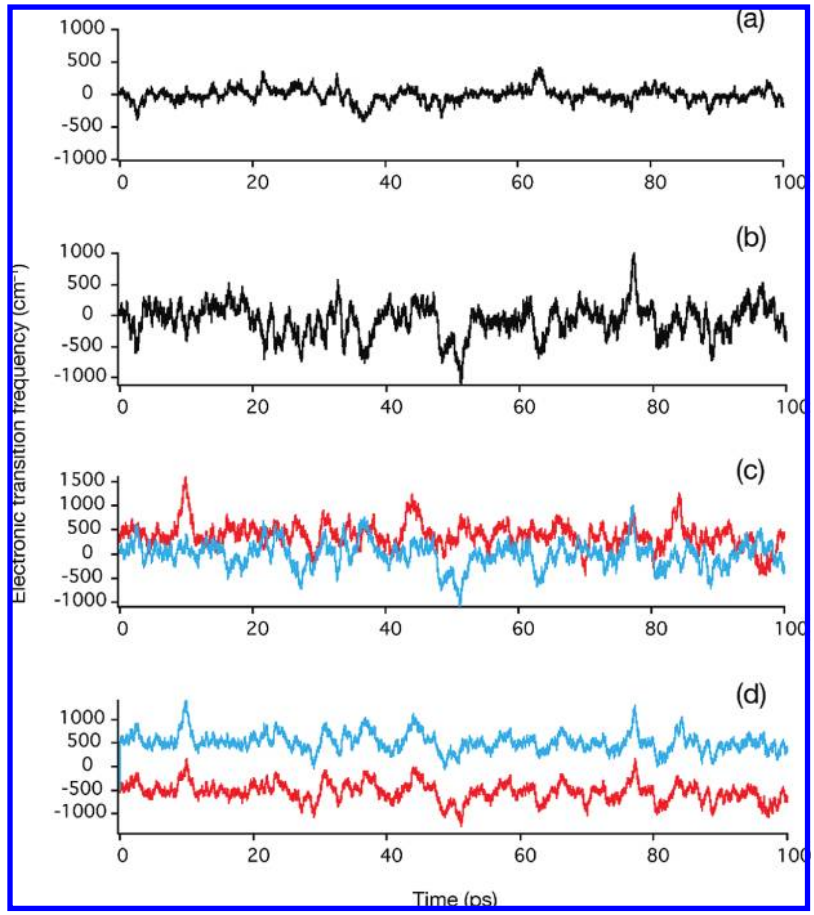

Figure 10. Calculations of the stochastic fluctuations in transition energy of a model chromophore coupled to a bath represented by an Ohmic spectral density. (a) A trajectory for a single molecule from the ensemble calculated for 100 K. (b) 300 K. (c) Calculation for two molecules (300 K) that are electronically coupled (see text). The zeroth-order energy difference between transitions on the two molecules is 400 cm^{-1}, and the electronic coupling is 5 cm^{-1}. (d) Same as the previous but with identical zeroth-order energies and an electronic coupling of 500 cm^{-1}.

We used a quantum-mechanical approach developed by Mennucci and co-workers[100,105] that solves the key aspect of the problem, as the solvent response to charge and, importantly, transition densities, is obtained by solving the Poisson equation in a realistic molecular-shaped cavity inside the dielectric environment. Solvent effects are described using the polarizable continuum model (PCM)[106] that consistently introduces their effect in all steps of the quantum-mechanical calculations: the evaluation of the excited states, the calculation of transition densities, and the interaction between molecules. We fitted our results (see Figure 9b) to an empirical distance-dependent screening function, averaged over multiple chromophores, shapes, and orientations:

$$s = A \exp(-\beta R) + s_0 \qquad (12)$$

where the pre-exponential factor is $A = 2.68$, the attenuation factor is $\beta = 0.27$, and $s_0 = 0.54$ is the asymptotic value of s at large distances. The protein medium was modeled with an optical dielectric constant $n^2 = 2$. The asymptotic value of s, $s_0 = 0.54$, falls in between the limits of the Förster model, $s_0 = 1/n^2 = 0.5$, and the Onsager model, $s_0 = 3/(2n^2 + 1) = 0.6$, owing to the effects of molecular shape.

7. Disorder, Ensemble Averages, and Single Molecule FRET

If we could watch the electronic transition energy as a function of time for a single molecule, we would see it fluctuate stochastically about a mean (see, e.g., ref 107). Examples are shown in Figure 10a,b of how an electronic transition ($0 \rightarrow e$) frequency for a single molecule ν_{e0} fluctuates at each of two different temperatures. These trajectories were calculated using a model Ohmic bath spectral density and a Markov chain procedure. In a real condensed phase system, we can measure the correlation function for those fluctuations $M(\tau) = \langle \nu_{e0}(\tau)\nu_{e0}(0)\rangle$, for example, using three-pulse photon echo peak shift or ultrafast measurements of the fluorescence Stokes shift.[108,109] We thereby find that there are multiple time scales of fluctuations in the nuclear coordinates that cause the transition energy fluctuations in the chromophores of interest. The time scales of energy gap fluctuations that occur faster than the experimental time scale (e.g., excited-state lifetime) lead to homogeneous line broadening.[70]

The spectral overlap in RET is a more complex kind of average because it relates the transition energy fluctuations on a donor chromophore to those of an acceptor chromophore. Here, in the weak electronic coupling limit, we need to think about a trajectory of transition energy fluctuations for each of the donors and acceptors and then determine the time-averaged probability that the energy gaps coincide. That is shown in Figure 10c, where the eigenstates of a weakly interacting donor−acceptor pair have been calculated at each time step in the simulation. The assumption underlying the simulation is that the transition energy fluctuations of the donor and acceptor are uncorrelated. The trajectory is color-coded to indicate the energy gap for each molecule, defined

by the magnitude of the coefficient in the eigenstate being greater than 0.8. We see that the two transition frequencies fluctuate independently. When they coincide or cross, excitation energy can hop from one molecule to the other while conserving energy. These crossing points therefore make the largest contribution to the spectral overlap when the ensemble average is taken. The amplitude of transition energy gap fluctuations is directly related to homogeneous line broadening in linear spectroscopies like absorption and fluorescence. That can be seen in the trajectories shown in Figure 10a,b. Thus, the probability of donor and acceptor trajectories crossing, and hence the spectral overlap, depends on temperature.

If we make some approximations about these stochastic modulations of the energy gap, then we can define a dephasing time that tells us how long it takes to sample the distribution of transition energies. This can be a useful guide, but as discussed above, restricting ourselves to such a simple view of the bath blinds us to many of the subtleties of non-Förster RET. For example, any fluctuations that are correlated on donor and acceptor contribute to the line width and dephasing time of each chomophore individually, just like any other fluctuation. However, as described in the previous section, because they do not increase the donor−acceptor energy mismatch, they do not contribute to the spectral overlap.

Such a situation of correlated fluctuations is found when the electronic coupling between the donor and acceptor molecules is large compared to the amplitude of the fluctuations, Figure 10d. Now the two trajectories do not cross at all. Relaxation among these two eigenstates does, nonetheless, occur. If the energy splitting is reasonably large, then the mechanism will involve high frequency intramolecular vibrations, as for a normal radiationless transition. Otherwise, it can occur by weak coupling to the bath. For that to be possible, there must be fluctuations of the bath that affect the eigenstates in a slightly different way, for example, because the change in dipole moment upon excitation of each eigenstate differs. Then, certain bath fluctuations, which we can consider to act with the length scale of the dimer rather than a single monomer, break the correlation among the eigenstates. Another observation from this simulation is that the amplitude of the fluctuations is reduced compared to those in the weak coupling case of Figure 10c. That phenomenon is usually called exchange (or spectral) narrowing, and it is caused by the eigenstate averaging over the fluctuations on the sites.[110] In long aggregates, a spectral line shape results that is significantly narrower than that for the isolated monomer.

In a single molecule fluorescence experiment, we can measure the homogeneous line shape individually for many chromophores in the ensemble, and it is found that each chromophore has a unique mean electronic transition energy.[111−113] This is caused by fluctuations of the nuclear degrees of freedom on time scales much longer than the experiment. The distribution of mean single molecule transition energies is typically Gaussian and contributes inhomogeneous broadening, or static disorder, to the ensemble spectra. In multichromophoric systems, we call this static disorder or *diagonal disorder* because the site energies in our Hamiltonian (the diagonal matrix elements) can take a distribution of energies.

Similarly, we can imagine a structural disorder in the system that leads to a distribution of donor−acceptor separations and/or orientations. This leads to a distribution in electronic couplings, called *off-diagonal disorder*. Identifying disorder versus homogeneous line broadening is crucial for quantifying spectral overlaps (actually, coupling-weighted spectral overlaps) in mutichromophoric donor−acceptor systems because we must calculate spectral overlaps using homogeneous line broadening and then average the electronic coupling−spectral overlap function over static disorder.[114]

7.1. Off-Diagonal Disorder. Consider a FRET experiment in which the donor and acceptor moieties are connected by a linker, and the resultant dyad molecules dissolved in a condensed phase. In general, each dyad will reside in its own unique environment and may even have its own unique structure and structural constraints determined by that environment. The ensemble spectrum will be inhomogeneously broadened, since each donor−acceptor pair will have (slightly) different energy levels. If a standard FRET experiment is carried out by exciting at a particular frequency, the results will be an average of the subensemble of dyads that absorb at that frequency. Interpreting the results in the normal manner will lead to an efficiency of FRET that may vary with exciting frequency. If the variation is large, the origin of the trend may be difficult to interpret. Even if the variation is not large, interesting effects may require a generalization of the FRET formula.

A recently reported FRET experiment of a dyad synthesized so that the angular factor, κ, is zero for the rigid molecule showed robust energy transfer.[115] This can be explained by invoking a torsional mode of the dyad about the linker that leads to an average of κ^2 that is nonzero.[116] Or it can be explained by environmentally induced structural disorder among the dyads.

If a single molecule FRET experiment is carried out by exciting a single donor, then there is no average over the inhomogeneous distribution. If the standard FRET formula applies (i.e., so that the various issues discussed in this paper do not apply), the distribution of results on many single molecules may be interpreted in terms of a distribution in distances, R, and angular factors, κ^2. That is, each dyad will have different values of the structural parameters and the experimenter will find a distribution of these that fits the experimental results.

If any of the issues raised in the present account are important, even single molecule FRET experiments on closely coupled dyads may be difficult to interpret. However, since the single molecule experiments avoid averaging, there will be a reasonable chance of extracting information on whether there are shared vibrations, differential solvent screening, coherences, etc.[117] It is evident that a clear interpretation can only be found by combining detailed theoretical calculations with experiment.

7.2. Diagonal Disorder. Diagonal disorder—a distribution of energies at each site in a molecular assembly—has been considered in a wide variety of systems. We suggest that the interested reader refer to the paper by Fidder et al. for a lucid introduction to the relationships between diagonal disorder and spectroscopy in molecular aggregates formed by self-assembled dye molecules.[118] One particular system that has attracted a great deal of attention over the past decade is the peripheral light-harvesting complex LH2 from purple photosynthetic bacteria. Peripheral antenna systems of various kinds are employed by photosynthetic organisms to increase the spatial and spectral cross section for light absorption.[119,120] They have proven to be superb model systems for learning about the mechanism and dynamics of RET in complex, but structurally well-defined, multichromophoric systems. There are several insightful reviews that introduce the structure−function relationships elucidated for LH2.[22,121−126]

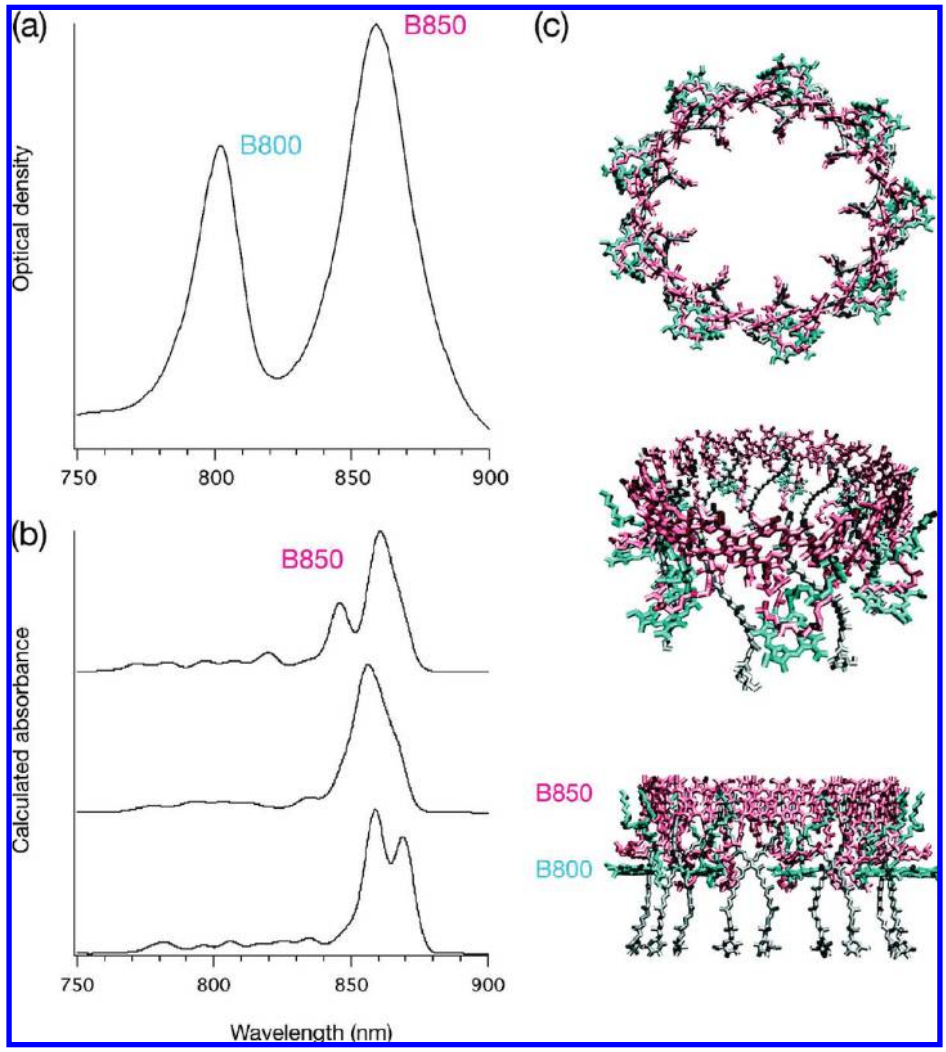

Figure 11. (a) Experimental absorption spectrum of the LH2 light-harvesting complex isolated from the purple bacterium *Rps. acidophila* (room temperature). The B800 and B850 bands are labeled. (b) Calculated absorption spectra of the B850 ring only for individual LH2 complex (77 K).[114] Notice that each complex is different. (c) Views of the LH2 structure.[129] The 18 bacteriochlorophyll-*a* molecules that comprise the B850 ring are colored pink, while the 9 in the B800 ring are blue. The carotenoids (rhodopin glucoside) are colored gray.

Early spectroscopic studies provided evidence, for example, from the spectral dependence of picosecond fluorescence decays, that inhomogeneity (disorder) is a central feature of LH2 photophysics.[127,128] A turning point came when Cogdell and co-workers solved the crystal structure for the LH2 antenna isolated from a strain of the organism *Rhodopseudomonas acidophila*, revealing the exquisite circular structure of this pigment−protein complex, Figure 11.[129] That structural model inspired a surge of papers. In particular, more quantitative conclusions could be drawn about the role and nature of disorder in these complexes.[114,130−143] A key finding of that work is how disorder localizes the excitation; that is, it reduces the coherence length of excitations in the B850 ring. The delocalization depends also on homogeneous line broadening dynamics, so different results are found, for example, for pump−probe spectroscopy at very short delay time compared to superradiance, which probes the fully equilibrated excited state.

Single molecule fluorescence experiments show very clearly how to think about disorder in the B850 ring.[144−149] In each LH2 protein complex, the local environment around each bacteriochlorophyll chromophore is slightly different. For example, local fluctuations in electrostatic environment and specific interactions, like hydrogen bonds, influence the site energies in ways that change slowly with time compared to the excited-state lifetime.[150−152] After accounting for the local site disorder in the bacteriochlorophyll transition energies and the electronic interactions among all of the bacteriochlorophylls in the ring, the exciton states that reflect that disorder are obtained. The resulting absorption spectra, calculated for individual LH2 complexes, are shown in Figure 11b. Note that each complex is unique, and that is evident in its absorption spectrum.[114]

An important implication of the disorder in the B850 ring is its effect on the mechanism and rate of B800-to-B850 RET. Depending on the species of purple bacteria, excitation energy is funneled from a largely localized state on the B800 ring to the B850 ring in approximately 0.7−0.8 ps at room temperature.[153−155] FRET theory predicts a significantly slower rate. It is a combination of GFT (see section 5.1) and correct averaging over disorder to obtain the spectral overlap that together allows quantitative explanation of the B800−B850 RET rate.[114] A recent report includes more details, such as coherence within each of the donor and acceptor rings and the multichromophoric nature of the B800 ring.[156] Results from that work are plotted in Figure 12. The main message in this figure is that FRET theory predicts a narrow distribution of B800−B850 rates for the LH2 ensemble, that are on average too slow compared to the experimental data. In contrast, GFT with disorder predicts

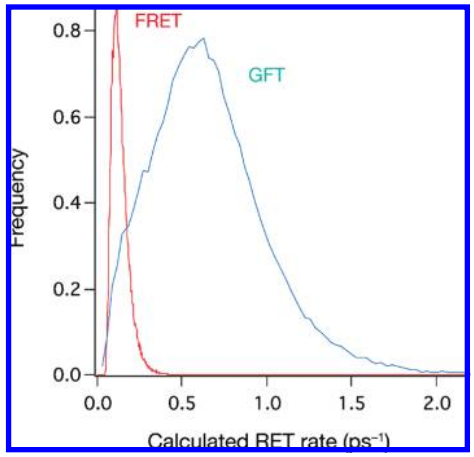

Figure 12. Calculated distributions of rates, i.e., calculated for each LH2 complex in an ensemble. The red curve is the FRET distribution. The blue curve shows the calculations of Jang et al. using a version of GFT.[156]

a broad distribution of rates, which on average are similar to the experimental data. The calculated rate is significantly faster than the FRET prediction because the most effective acceptor states are the dark B850 exciton transitions that lie in resonance with the B800 emission spectrum.[114]

8. Conclusions and Outlook

The usual formulation of Förster's theory of resonance energy transfer is highly successful in many instances. Nonetheless, as we examine its ingredients more closely, there are several interesting ways that it can break down, leading to mechanisms beyond Förster theory for mediating resonance energy transfer. These non-Förster phenomena are interesting from both theoretical and experimental viewpoints because they challenge our understanding of dynamics promoted by quantum-mechanical interactions. For example, we have learned how electronic interactions between donors and acceptors resolve details of molecular shape in a way that spectroscopy does not. Furthermore, even solvent screening of the electronic coupling depends to some extent on donor and acceptor shape. More sophisticated concepts underlie the recent observations of electronic coherence in energy transfer dynamics. In some cases, it is evident that simple descriptions of the nuclear bath—like the decoherence time—do not convey enough detail to provide an understanding of how the length scale, origin, and correlation of nuclear motions dictate the coupling among chromophores. Future work will be needed to elucidate incredibly detailed descriptions of the interplay between electronic coupling and bath fluctuations in order to capture the local picture of environment-induced decoherence around each chromophore.

Acknowledgment. The work in Toronto was supported by the Natural Sciences and Engineering Research Council of Canada. G.D.S. acknowledges the support of an E. W. R. Steacie Memorial Fellowship. The work in Mons was supported by the European Commission through the EC STREP project MODECOM (NMP-CT-2006-016434) and the Belgian National Science Foundation (FNRS). D.B. is a Research Director of the FNRS. The work at MIT was supported by NSF grant CHE0556268.

References and Notes

(1) Van Der Meer, B. W.; Coker, G.; Chen, S.-Y. S. *Resonance Energy Transfer: Theory and Data*; VCH: New York, 1994.
(2) Scholes, G. D. *Annu. Rev. Phys. Chem.* **2003**, *54*, 57–87.
(3) Kallmann, H.; London, F. *Z. Phys. Chem.* **1929**, *2*, 207–243.
(4) Vavilov, A. C. H.; Galanin, M. D. *Dokl. Akad. Nauk USSR* **1949**, *67*, 811–818.
(5) Förster, T. *Ann. Phys.* **1948**, *2*, 55–75.
(6) Agabekyan, A. S.; Melikyan, A. O. *Opt. Spectrosc.* **1972**, *32*, 153–157.
(7) Kasha, M. *Radiat. Res.* **1963**, *20*, 55.
(8) May, V.; Kühn, O. *Charge and energy transfer dynamics in molecular systems: A theoretical introduction*; Wiley-VCH: Berlin, 2000.
(9) Braslavsky, S. E.; Fron, E.; Rodriguez, H. B.; San Román, E.; Scholes, G. D.; Schweitzer, G.; Valeur, B.; Wirz, J. *Photochem. Photobiol. Sci.* **2008**, *7*, 1444–1448.
(10) Andrews, D. L. *Chem. Phys.* **1989**, *135*, 195–201.
(11) Craig, D. P.; Thirunamachandran, T. *Molecular Quantum Electrodynamics*; Dover: New York, 1998.
(12) Krueger, B. P.; Scholes, G. D.; Fleming, G. R. *J. Phys. Chem. B* **1998**, *102*, 5378–5386.
(13) Walla, P. J.; Linden, P. A.; Hsu, C. P.; Scholes, G. D.; Fleming, G. R. *Proc. Natl. Acad. Sci. U.S.A.* **2000**, *97*, 10808–10813.
(14) Tretiak, S.; Mukamel, S. *Chem. Rev.* **2002**, *102*, 3171.
(15) Chang, J. C. *J. Chem. Phys.* **1977**, *67*, 3901–3909.
(16) Beljonne, D.; Cornil, J.; Silbey, R.; Millie, P.; Brédas, J.-L. *J. Chem. Phys.* **2000**, *112*, 4749–4758.
(17) Czikklely, V.; Fosterling, H. D.; Kuhn, H. *Chem. Phys. Lett.* **1970**, *6*, 207–210.
(18) Beenken, W. J. D.; Pullerits, T. *J. Chem. Phys.* **2004**, *120*, 2490–2495.
(19) Fink, R. F.; Pfister, J.; Schneider, A.; Zhao, H.; Engles, B. *Chem. Phys.* **2008**, *343*, 353–361.
(20) Fink, R. F.; Pfister, J.; Zhao, H. M.; Engels, B. *Chem. Phys.* **2008**, *346*, 275–285.
(21) Muñoz-Losa, A.; Curutchet, C.; Galván, I. F.; Mennucci, B. *J. Chem. Phys.* **2008**, *129*, 034104.
(22) Scholes, G. D.; Fleming, G. R. *Adv. Chem. Phys.* **2005**, *132*, 57–130.
(23) Beljonne, D.; Pourtois, G.; Silva, C.; Hennebicq, E.; Herz, L. M.; Friend, R. H.; Scholes, G. D.; Setayesh, S.; Müllen, K.; Brédas, J. L. *Proc. Natl. Acad. Sci. U.S.A.* **2002**, *99*, 10982–10987.
(24) Peeters, E.; van Hal, P. A.; Knol, J.; Brabec, C. J.; Sariciftci, N. S.; Hummelen, J. C.; Janssen, R. A. J. *J. Phys. Chem. B* **2000**, *104*, 10174–10190.
(25) van Hal, P. A.; Janssen, R. A. J.; Lanzani, G.; Cerullo, G.; Zavelani-Rossi, M.; De Silvestri, S. *Phys. Rev. B* **2001**, *64*, 075206.
(26) van Hal, P. A.; Janssen, R. A. J.; Lanzani, G.; Cerullo, G.; Zavelani-Rossi, M.; De Silvestri, S. *Chem. Phys. Lett.* **2001**, *345*, 33–38.
(27) Gonzalez-Rodriguez, D.; Torres, T.; Guldi, D. M.; Rivera, J.; Echegoyen, L. *Org. Lett.* **2002**, *4*, 335–338.
(28) Gayathri, S. S.; Patnaik, A. *Chem. Phys. Lett.* **2005**, *414*, 198–203.
(29) Lloyd, M. T.; Lim, Y.-F.; Malliaras, G. G. *Appl. Phys. Lett.* **2008**, *92*, 143308.
(30) Hukka, T. I.; Toivonen, T.; Hennebicq, E.; Brédas, J.-L.; Janssen, R. A. J.; Beljonne, D. *Adv. Mater.* **2006**, *18*, 1301–1306.
(31) Scholes, G. D.; Gould, I. R.; Cogdell, R. J.; Fleming, G. R. *J. Phys. Chem. B* **1999**, *103*, 2543–2553.
(32) Wiesenhofer, H.; Beljonne, D.; Scholes, G. D.; Hennebicq, E.; Brédas, J.-L.; Zojer, E. *Adv. Funct. Mater.* **2005**, *15*, 155–160.
(33) Wong, K. F.; Bagchi, B.; Rossky, P. J. *J. Phys. Chem. A* **2004**, *108*, 5752–5763.
(34) Scholes, G. D.; Andrews, D. L. *Phys. Rev. B* **2005**, *72*, 125331.
(35) Kagan, C. R.; Murray, C. B.; Nirmal, M.; Bawendi, M. G. *Phys. Rev. Lett.* **1996**, *76*, 1517.
(36) Medintz, I. L.; Clapp, A. R.; Mattoussi, H.; Goldman, E. R.; Fisher, B.; Mauro, J. M. *Nat. Mater.* **2003**, *2*, 630–638.
(37) Medintz, I. L.; Mattoussi, H. *Phys. Chem. Chem. Phys.* **2009**, *11*, 17–45.
(38) O'Connell, M. J.; Bachilo, S. M.; Huffman, C. B.; Moore, V. C.; Strano, M. S.; Haroz, E. H.; Rialon, K. L.; Boul, P. J.; Noon, W. H.; Kittrell, C.; Ma, J.; Hauge, R. H.; Weisman, R. B.; Smalley, R. E. *Science* **2002**, *297*, 593–596.
(39) Curutchet, C.; Franceschetti, A.; Zunger, A.; Scholes, G. D. *J. Phys. Chem. C* **2008**, *112*, 13336–13341.
(40) Wong, C. Y.; Curutchet, C.; Tretiak, S.; Scholes, G. D. *J. Chem. Phys.* **2009**, *130*, 081104.
(41) Wang, L.-W.; Zunger, A. *Phys. Rev. B* **1995**, *51*, 17398–17416.
(42) Schrier, J.; Wang, L.-W. *J. Phys. Chem. C* **2008**, *112*, 11158–11161.
(43) Closs, G. L.; Piotrowiak, P.; MacInnes, J. M.; Fleming, G. R. *J. Am. Chem. Soc.* **1988**, *110*, 2652–2653.
(44) Naleway, C. A.; Curtiss, L. A.; Miller, J. R. *J. Phys. Chem.* **1991**, *95*, 8434–8437.

(45) Paulson, B. P.; Curtiss, L. A.; Bal, B.; Closs, G. L.; Miller, J. R. *J. Am. Chem. Soc.* **1996**, *118*, 378–387.
(46) Jordan, K. D.; Paddon-Row, M. N. *Chem. Rev.* **1992**, *92*, 395–410.
(47) Oevering, H.; Paddon-Row, M. N.; Heppener, M.; Oliver, A. M.; Cotsaris, E.; Verhoeven, J. W.; Hush, N. S. *J. Am. Chem. Soc.* **1987**, *109*, 3258–3269.
(48) Paddon-Row, M. N. *Aust. J. Chem.* **2003**, *56*, 729–748.
(49) Scholes, G. D.; Ghiggino, K. P. *J. Phys. Chem.* **1994**, *98*, 4580–4590.
(50) Eng, M. P.; Albinsson, B. *Angew. Chem., Int. Ed.* **2006**, *45*, 5626–5629.
(51) Albinsson, B.; Mårtensson, J. *J. Photochem. Photobiol., C* **2008**, *9*, 138–155.
(52) Eng, M. P.; Mårtensson, J.; Albinsson, B. *Chem.—Eur. J.* **2008**, *14*, 2819–2826.
(53) Scholes, G. D.; Harcourt, R. D.; Ghiggino, K. P. *J. Chem. Phys.* **1995**, *102*, 9574–9581.
(54) Thompson, A. L.; Gaab, K. M.; Xu, J.; Bardeen, C. J.; Martinez, T. J. *J. Phys. Chem. A* **2004**, *108*, 671–682.
(55) Van Averbeke, B.; Beljonne, D.; Hennebicq, E. *Adv. Funct. Mater.* **2008**, *18*, 492–498.
(56) Clayton, A. H. A.; Scholes, G. D.; Ghiggino, K. P.; Paddon-Row, M. N. *J. Phys. Chem.* **1996**, *100*, 10912–10918.
(57) Métivier, R.; Nolde, F.; Müllen, K.; Basché, T. *Phys. Rev. Lett.* **2007**, *98*, 47802.
(58) Curutchet, C.; Mennucci, B.; Scholes, G. D.; Beljonne, D. *J. Phys. Chem. B* **2008**, *112*, 3759–3766.
(59) Lee, H.; Cheng, Y.-C.; Fleming, G. R. *Science* **2007**, *316*, 1462–1465.
(60) Engel, G. S.; Calhoun, T. R.; Read, E. L.; Ahn, T.-K.; Mancal, T.; Cheng, Y.-C.; Blankenship, R. E.; Fleming, G. R. *Nature (London)* **2007**, *446*, 782–786.
(61) Collini, E.; Scholes, G. D. *Science* **2009**, *323*, 369–373.
(62) Note that the final column in Table 1 in ref 2 needs correction: The couplings reported for the distributed dipole approximation are in error for the interchromophore separations described. The following substitutions should be made: $V = 3.2 \rightarrow 1.4$; $2.5 \rightarrow 19$; $8.3 \rightarrow -8.3$; $5.6 \rightarrow -5.6$. G.D.S. is grateful to B. Kohler for pointing this out.
(63) Sumi, H. *J. Phys. Chem. B* **1999**, *103*, 252–260.
(64) Scholes, G. D.; Jordanides, X. J.; Fleming, G. R. *J. Phys. Chem. B* **2001**, *105*, 1640–1651.
(65) Jang, S.; Newton, M. D.; Silbey, R. J. *Phys. Rev. Lett.* **2004**, *92*, 218301.
(66) Jordanides, X. J.; Scholes, G. D.; Fleming, G. R. *J. Phys. Chem. B* **2001**, *105*, 1652–1669.
(67) Marcus, R. A.; Sutin, N. *Biochim. Biophys. Acta* **1985**, *811*, 265–322.
(68) Mirkovic, T.; Doust, A. B.; Kim, J.; Wilk, K. E.; Curutchet, C.; Mennucci, B.; Cammi, R.; Curmi, P. M. G.; Scholes, G. D. *Photochem. Photobiol. Sci.* **2007**, *6*, 964–975.
(69) Mukamel, S. *Principles of Nonlinear Optical Spectroscopy*; Oxford University Press: New York, 1995.
(70) Fleming, G. R.; Passino, S. A.; Nagasawa, Y. *Philos. Trans. R. Soc. London, Ser. A* **1998**, 356–389.
(71) Scholes, G. D.; Ghiggino, K. P. *J. Chem. Phys.* **1994**, *101*, 1251–1261.
(72) Jang, S.; Jung, Y. J.; Silbey, R. *J. Chem. Phys.* **2002**, *275*, 319–332.
(73) Fulton, R. L.; Gouterman, M. *J. Chem. Phys.* **1961**, *35*, 1059–1071.
(74) Klafter, J.; Silbey, R. *Phys. Lett. A* **1980**, *76*, 143–146.
(75) Pope, M.; Swenberg, E. *Electronic Processes in Organic Crystals and Polymers*; 2nd ed.; Oxford Science Publications: New York, 1999.
(76) Pope, M.; Swenberg, C. E. *Annu. Rev. Phys. Chem.* **1984**, *35*, 613–655.
(77) McRae, E. G.; Kasha, M. *Physical Processes in Radiation Biology*; Academic Press: New York, 1964; pp 23−42.
(78) Heijs, D. J.; Malyshev, V. A.; Knoester, J. *Phys. Rev. Lett.* **2005**, *95*, 177402.
(79) Bednarz, M.; Malyshev, V. A.; Knoester, J. *J. Chem. Phys.* **2002**, *117*, 6200–6213.
(80) Didraga, C.; Malyshev, V. A.; Knoester, J. *J. Phys. Chem. B* **2006**, *110*, 18818–18827.
(81) Rackovsky, S.; Silbey, R. *Mol. Phys.* **1973**, *25*, 61–72.
(82) Grover, M.; Silbey, R. *J. Chem. Phys.* **1971**, *54*, 4843–4851.
(83) Jackson, B.; Silbey, R. *J. Chem. Phys.* **1983**, *78*, 4193–4196.
(84) Kimura, A.; Kakitani, T. *J. Phys. Chem. A* **2007**, *111*, 12042–12048.
(85) Kimura, A.; Kakitani, T. *J. Phys. Chem. B* **2003**, *107*, 14486–14499.
(86) Suarez, A.; Silbey, R.; Oppenheim, I. *J. Chem. Phys.* **1992**, *97*, 5101–5107.
(87) Fleming, G. R. *Chemical applications of ultrafast spectroscopy*; Oxford University Press: New York, 1986.
(88) Jonas, D. M. *Annu. Rev. Phys. Chem.* **2003**, *54*, 425–463.
(89) Jonas, D. M. *Science* **2003**, *300*, 1515–1517.
(90) Cho, M. *Chem. Rev.* **2008**, *108*, 1331–1418.
(91) Pisliakov, A. V.; Mancal, T.; Fleming, G. R. *J. Chem. Phys.* **2006**, *124*, 234505.
(92) Cho, M. H.; Vaswani, H. M.; Brixner, T.; Stenger, J.; Fleming, G. R. *J. Phys. Chem. B* **2005**, *109*, 10542–10556.
(93) Brixner, T.; Stenger, J.; Vaswani, H. M.; Cho, M.; Blankenship, R. E.; Fleming, G. R. *Nature (London)* **2005**, *434*, 625–628.
(94) Zigmantas, D.; Read, E. L.; Mancal, T.; Brixner, T.; Gardiner, A. T.; Cogdell, R. J.; Fleming, G. R. *Proc. Natl. Acad. Sci. U.S.A.* **2006**, *103*, 12672–12677.
(95) Cheng, Y. C.; Engel, G. S.; Fleming, G. R. *Chem. Phys.* **2007**, *341*, 285–295.
(96) Cheng, Y. C.; Fleming, G. R. *J. Phys. Chem. A* **2008**, *112*, 4254–4260.
(97) Agranovich, V. M.; Galanin, M. D. *Electronic Excitation Transfer in Condensed Matter*; North-Holland: Amsterdam, 1982.
(98) Juzeliunas, G.; Andrews, D. L. *Phys. Rev. B* **1994**, *49*, 8751.
(99) Hsu, C.-P.; Fleming, G. R.; Head-Gordon, M.; Head-Gordon, T. *J. Chem. Phys.* **2001**, *114*, 3065–3072.
(100) Iozzi, M. F.; Mennucci, B.; Tomasi, J.; Cammi, R. *J. Chem. Phys.* **2004**, *120*, 7029–7040.
(101) Adolphs, J.; Renger, T. *Biophys. J.* **2006**, *91*, 2778.
(102) Knox, R. S.; van Amerongen, H. *J. Phys. Chem. B* **2002**, *106*, 5289–5293.
(103) Scholes, G. D.; Curutchet, C.; Mennucci, B.; Cammi, R.; Tomasi, J. *J. Phys. Chem. B* **2007**, *111*, 6978–6982.
(104) Curutchet, C.; Scholes, G. D.; Mennucci, B.; Cammi, R. *J. Phys. Chem. B* **2007**, *111*, 13253–13265.
(105) Curutchet, C.; Mennucci, B. *J. Am. Chem. Soc.* **2005**, *127*, 16733–16744.
(106) Tomasi, J.; Mennucci, B.; Cammi, R. *Chem. Rev.* **2005**, *105*, 2999–3093.
(107) Mercer, I. P.; Gould, I. R.; Klug, D. R. *J. Phys. Chem. B* **1999**, *103*, 7720–7727.
(108) Fleming, G. R.; Cho, M. H. *Annu. Rev. Phys. Chem.* **1996**, *47*, 109–134.
(109) Maroncelli, M. *J. Mol. Liq.* **1993**, *57*, 1–37.
(110) Kubo, R. *Adv. Chem. Phys.* **1969**, *15*, 101–127.
(111) Moerner, W. E. *J. Phys. Chem. B* **2002**, *106*, 910–927.
(112) Silbey, R. J. *Proc. Natl. Acad. Sci. U.S.A.* **2007**, *104*, 12595–12595.
(113) De Schryver, F. C.; Vosch, T.; Cotlet, M.; Van der Auweraer, M.; Müllen, K.; Hofkens, J. *Acc. Chem. Res.* **2005**, *38*, 514–522.
(114) Scholes, G. D.; Fleming, G. R. *J. Phys. Chem. B* **2000**, *104*, 1854–1868.
(115) Langhals, H.; Poxleitner, S.; Krotz, O.; Pust, T.; Walter, A. *Eur. J. Org. Chem.* **2008**, 4559–4562.
(116) Jang, S. *J. Chem. Phys.* **2007**, *127*, 174710.
(117) Barkai, E.; Jung, Y. J.; Silbey, R. *Annu. Rev. Phys. Chem.* **2004**, *55*, 457–507.
(118) Fidder, H.; Knoester, J.; Wiersma, D. A. *J. Chem. Phys.* **1991**, *95*, 7880–7890.
(119) Duysens, L. N. M. In *Light emission by plants and bacteria*; Govindjee Amesz, J., Fork, D. C., Eds.; Academic Press, Inc.: Orlando, FL, 1986; pp 3−28.
(120) van Grondelle, R. *Biochim. Biophys. Acta* **1985**, *811*, 147–195.
(121) Pullerits, T.; Sundström, V. *Acc. Chem. Res.* **1996**, *29*, 381–389.
(122) Fleming, G. R.; van Grondelle, R. *Curr. Opin. Struct. Biol.* **1997**, *7*, 738–748.
(123) Sundström, V.; Pullerits, T.; van Grondelle, R. *J. Phys. Chem. B* **1999**, *103*, 2327–2346.
(124) Hu, X.; Damjanovic, A.; Ritz, T.; Schulten, K. *Proc. Natl. Acad. Sci. U.S.A.* **1998**, *95*, 5935–5941.
(125) van Grondelle, R.; Novoderezhkin, V. *Biochemistry* **2001**, *40*, 15057–15068.
(126) Cogdell, R. J.; Gardiner, A. T.; Roszak, A. W.; Law, C. J.; Southall, J.; Isaacs, N. W. *Photosynth. Res.* **2004**, *81*, 207–214.
(127) Freiberg, A.; Godik, V. I.; Pullerits, T.; Timpmann, K. *Biochim. Biophys. Acta* **1989**, *973*, 93–104.
(128) Pullerits, T.; Freiberg, A. *Chem. Phys.* **1991**, *149*, 409–418.
(129) McDermott, G.; Prince, S. M.; Freer, A. A.; Hawthornthwaite-Lawless, A. M.; Papiz, M. Z.; Cogdell, R. J.; Isaacs, N. W. *Nature (London)* **1995**, *374*, 517–521.
(130) Sauer, K.; Cogdell, R. J.; Prince, S. M.; Freer, A. A.; Isaacs, N. W.; Scheer, H. *Photochem. Photobiol.* **1996**, *64*, 564–576.
(131) Pullerits, T.; Chachisvilis, M.; Sundström, V. *J. Phys. Chem.* **1996**, *100*, 10787–10792.
(132) Jimenez, R.; Dikshit, S. N.; Bradforth, S. E.; Fleming, G. R. *J. Phys. Chem.* **1996**, *100*, 6825–6834.
(133) Wu, H.-M.; Savikhin, S.; Reddy, N. R. S.; Jankowiak, R.; Cogdell, R. J.; Struve, W. S.; Small, G. J. *J. Phys. Chem.* **1996**, *100*, 12022–12033.
(134) Monshouwer, R.; Abrahamsson, M.; van Mourik, F.; van Grondelle, R. *J. Phys. Chem. B* **1997**, *101*, 7241–7248.

(135) Meier, T.; Chernyak, V.; Mukamel, S. *J. Phys. Chem. B* **1997**, *101*, 7332–7342.
(136) Wu, H.-M.; Ratsep, M.; Lee, I.-J.; Cogdell, R. J.; Small, G. J. *J. Phys. Chem. B* **1997**, *101*, 7654–7663.
(137) Kumble, R.; Hochstrasser, R. M. *J. Chem. Phys.* **1998**, *109*, 855–865.
(138) Freiberg, A.; Timpmann, K.; Lin, S.; Woodbury, N. W. *J. Phys. Chem. B* **1998**, *102*, 10974–10982.
(139) Nagarajan, V.; Johnson, E. T.; Williams, J. C.; Parson, W. W. *J. Phys. Chem. B* **1999**, *103*, 2297–2309.
(140) Bakalis, L. D.; Knoester, J. *J. Phys. Chem. B* **1999**, *103*, 6620–6628.
(141) Novoderezhkin, V.; Monshouwer, R.; van Grondelle, R. *J. Phys. Chem. B* **1999**, *103*, 10540–10548.
(142) Jang, S.; Dempster, S. E.; Silbey, R. J. *J. Phys. Chem. B* **2001**, *105*, 6655–6665.
(143) Zerlauskiene, O.; Trinkunas, G.; Gall, A.; Robert, B.; Urboniene, V.; Valkunas, L. *J. Phys. Chem. B* **2008**, *112*, 15883–15892.
(144) van Oijen, A. M.; Ketelaars, M.; Köhler, J.; Aartsma, T. J.; Schmidt, J. *Science* **1999**, *285*, 400–402.
(145) Ketelaars, M.; van Oijen, A. M.; Matsushita, M.; Ḱ; ohler, J.; Schmidt, J.; Aartsma, T. J. *Biophys. J.* **2001**, *80*, 1591–1603.
(146) Cogdell, R. J.; Gall, A.; Köhler, J. *Q. Rev. Biophys.* **2006**, *39*, 227–324.
(147) Ketelaars, M.; Segura, J.-M.; Oellerich, S.; de Ruijter, W. P. F.; Magis, G.; Aartsma, T. J.; Matsushita, M.; Schmidt, J.; Cogdell, R. J.; Köhler, J. *J. Phys. Chem. B* **2006**, *110*, 18710–18717.
(148) Rutkauskas, D.; Novoderezhkin, V.; Gall, A.; Olsen, J.; Cogdell, R. J.; Hunter, C. N.; van Grondelle, R. *Biophys. J.* **2006**, *90*, 2475–2485.
(149) Jang, S.; Silbey, R. J. *J. Chem. Phys.* **2003**, *118*, 9324.
(150) Fowler, G.; Visschers, R.; Grief, G.; van Grondelle, R.; Hunter, C. N. *Nature (London)* **1992**, *355*, 848–850.
(151) Cogdell, R. J.; Howard, T. D.; Isaacs, N. W.; McLuskey, K.; Gardiner, A. T. *Photosynth. Res.* **2002**, *74*, 135–141.
(152) Janosi, L.; Kosztin, I.; Damjanovic, A. *J. Chem. Phys.* **2006**, *125*, 014903.
(153) Kennis, J. T. M.; Streltsov, A. M.; Aartsma, T. J.; Nozawa, T.; Amesz, J. *J. Phys. Chem.* **1996**, *100*, 2438–2442.
(154) Ma, Y.-Z.; Cogdell, R. J.; Gillbro, T. *J. Phys. Chem. B* **1997**, *101*, 1087–1095.
(155) Pullerits, T.; Hess, S.; Herek, J. L.; Sundström, V. *J. Phys. Chem. B* **1997**, *101*, 10560–10567.
(156) Jang, S.; Newton, M. D.; Silbey, R. J. *J. Phys. Chem. B* **2007**, *111*, 6807–6814.

JP900708F